minerals

MDPI

Article

Petrochronological Evidence for a Three-Stage Magmatic Evolution of the Youngest Nepheline Syenites from the Ditrău Alkaline Massif, Romania

Urs Klötzli [1,*], Jolanta Burda [2], Qiu-Li Li [3], Yu Liu [3], Gyula Jakab [4], Lucian Ionescu [5] and Paul Tibuleac [6]

1 Department of Lithospheric Research, University of Vienna, Josef-Holaubek-Platz 2, 1090 Vienna, Austria
2 Institute of Earth Sciences, Faculty of Natural Sciences, University of Silesia in Katowice, 41-200 Sosnowiec, Poland; jolanta.burda@us.edu.pl
3 State Key Laboratory of Lithospheric Evolution, Institute of Geology and Geophysics, Chinese Academy of Sciences, Beijing 100029, China; liqiuli@mail.iggcas.ac.cn (Q.-L.L.); liuyu@mail.iggcas.ac.cn (Y.L.)
4 Mineral Land, Strada Spitalului 6, 535500 Gheorgheni, Romania; drjakabgy@yahoo.com
5 Romanian Waters National Administration Olt Water Directorate, Strada Progresului 16, 530240 Miercurea Ciuc, Romania; lucian.ionescu@gmail.com
6 Department of Geology, University Alexandru Ioan Cuza of Iasi, Boulevard Carol I, 20 A, 700506 Iasi, Romania; paul.tibuleac@uaic.ro
* Correspondence: urs.kloetzli@univie.ac.at

check for updates

Citation: Klötzli, U.; Burda, J.; Li, Q.-L.; Liu, Y.; Jakab, G.; Ionescu, L.; Tibuleac, P. Petrochronological Evidence for a Three-Stage Magmatic Evolution of the Youngest Nepheline Syenites from the Ditrău Alkaline Massif, Romania. *Minerals* **2022**, *12*, 657. https://doi.org/10.3390/min12050657

Academic Editor: Anastassia Yurievna Borisova

Received: 5 April 2022
Accepted: 18 May 2022
Published: 23 May 2022

Abstract: The Ditrău Alkaline Massif (DAM) is an igneous massif in the Eastern Carpathian Mountains of Romania. Numerous geochronological and geochemical studies have proposed a long formation history (ca. 70 m.y.) of the DAM from Middle Triassic to Cretaceous times, which is hardly reconcilable with geochemical evolutionary models and the geotectonic environment during the Mesozoic in this part of the Eastern Carpathian Mountains. In order to put tighter age constraints on the igneous processes forming the DAM, two nepheline syenites from the so-called Ghiduţ and Lăzarea suites were investigated. Based on field and geochemical evidence, the two rock suites represent the younger part of the DAM intrusives. Detailed zircon characterization, in situ zircon SIMS U-Pb dating, and geochemical modelling were used to establish the timing of zircon crystallization and thus to set time constraints on the igneous formation of these parts of the DAM. The intrusion of the dated Ghiduţ suite sample took place at 232 $\pm$ 1 Ma in the Karnium, whereas the Lăzarea suite nepheline syenite sample was intruded at 225 $\pm$ 1 Ma in the Norium. Together with published geochemical and geochronological data, three different magmatic events can thus be identified: Ghiduţ suite at 231.1 $\pm$ 0.8 Ma, Ditrău suite at 230.7 $\pm$ 0.2 Ma, and Lăzarea suite at 224.9 $\pm$ 1.1 Ma. Although the ages of the events 1 and 2 are statistically indistinguishable, the combination of geochemical and petrochronological data certainly favor independent intrusion events. Thus, the igneous events forming the younger parts of the DAM encompassed a time span of ca. 13 m.y. Additionally, each igneous event can tentatively be divided in an older syenitic stage and a younger nepheline syenitic one, each with an age difference of some 100,000 years. No indication of any post 215 Ma igneous or hydrothermal activity was found. The new data and interpretation significantly improve our understanding of the temporal and geochemical evolution of the DAM and of alkaline complexes as such, demonstrating that the underlying igneous processes (melt generation, assimilation, fractionation, and the duration of plumbing systems) work on the same time scale for both sorts of magmatic rock suites.

Keywords: zircon petrochronology; Ditrău Alkaline Massif; Eastern Carpathians; syenite

1. Introduction

Alkaline rocks, in particular intrusive alkali complexes, although representing only a small fraction of all igneous rocks (<1%), cover an incredibly wide range of chemical and mineralogical compositions. The petrogenesis of these rocks is interesting not only because of their great variability reflecting numerous petrological and mineralogical processes, but also for economic reasons, as they contain most of the global reserves of the rare earth elements, Y, Nb, and Ta. However, the dynamics behind intrusive alkaline complexes, especially their chronological evolution (i.e., the longevity of heating sources, plumbing and storage systems, duration of igneous activity from first melt generation to late- and post-magmatic hydrothermal–metasomatic overprinting, temporal aspects of the geochemical and isotope geochemical evolution) remain largely enigmatic, especially compared to the huge data set and knowledge base on granitic and basaltic igneous systems. Although there exists a number of well-studied alkaline complexes with an extensive data set of absolute age data (e.g., [1–6]), none of them has revealed its temporal evolution in such detail as has been found for more silicic complexes (e.g., [7–9]). From a geochronological point of view, the main problem arises during the integration of accurate and precise absolute age data for specific geological events and processes with the alkali complex's evolution for the following reasons: (a) Highly fractionated alkaline and ultra-alkaline igneous rocks, especially of silica-undersaturated and/or ultrabasic composition, often do not contain significant amounts of minerals (e.g., zircon, phosphate minerals, titanite), which potentially can provide accurate and precise growth ages. On the other hand, classical mineral cooling ages gained from more abundant minerals in these rock types (e.g., micas, amphiboles) are often fallacious and geologically of doubtful value due to the open-system behavior of the mineral chronometers in question. (b) Alkaline igneous rocks typically show intensive late- to post-magmatic hydrothermal and metasomatic overprinting, thus obscuring a primary geochronological signal, again due to the open-system behavior of many geochronometers during such events.

Using in situ and in-context petrochronological tools, it is possible to overcome these restrictions. In situ and in-context dating methods, (i.e., SIMS (Secondary Ion Mass Spectrometry), LA-(MC)-ICP-MS (Laser-Ablation (Multi-Collector) Inductively-Coupled Plasma Mass Spectrometry), and EMPA (Electron Microprobe Analysis) U-Th-Pb dating) explicitly allow to target unaltered mineral domains in the 1 μm to 50 μm range for even strongly overprinted rocks, thus allowing to define geologically meaningful pre-overprinting age data sets (e.g., [10–13]). However, it is important to state that these tools are specifically addressing the absolute dating of mineral growth, and that they are not devised to provide classical mineral cooling ages such as are gained by $^{40}Ar/^{39}Ar$ or Rb/Sr mineral dating.

Here we report the first results of a petrochronological study of two metasomatically partially altered alkaline rocks from the youngest parts of the Ditrău Alkaline Massiv (DAM) in the Eastern Carpathian Mountains in Romania. Detailed zircon characterization, in situ zircon SIMS U-Pb dating, and geochemical modelling are used to establish the timing of zircon crystallization and thus to set time constraints on the igneous formation of these rocks. We present how a distinct three-stage magmatic evolution becomes evident, resulting in a significantly improved understanding of the temporal and geochemical evolution of the DAM.

2. Geological Background

2.1. Overview

The Ditrău Alkaline Massif (DAM) is an alkaline igneous massif in the Eastern Carpathian Mountains in Romania (Figure 1). It was emplaced in an extensional, rift-related continental intraplate setting connected to the opening of the Meliata-Hallstatt Ocean in the Middle to Upper Triassic [14]. The host rocks of the DAM are pre-Middle Triassic metamorphic rocks of the Bretila, Tulgheş, Negrişoara, and Rebra Nappes, all of which are now parts of the Alpine Bucovinian Nappe [15]. The DAM is partially covered by Neogene volcanics and Pliocene-Pleistocene lacustrine sediments [16,17] and cut by E–W to NE–SW trending fault systems [17,18].

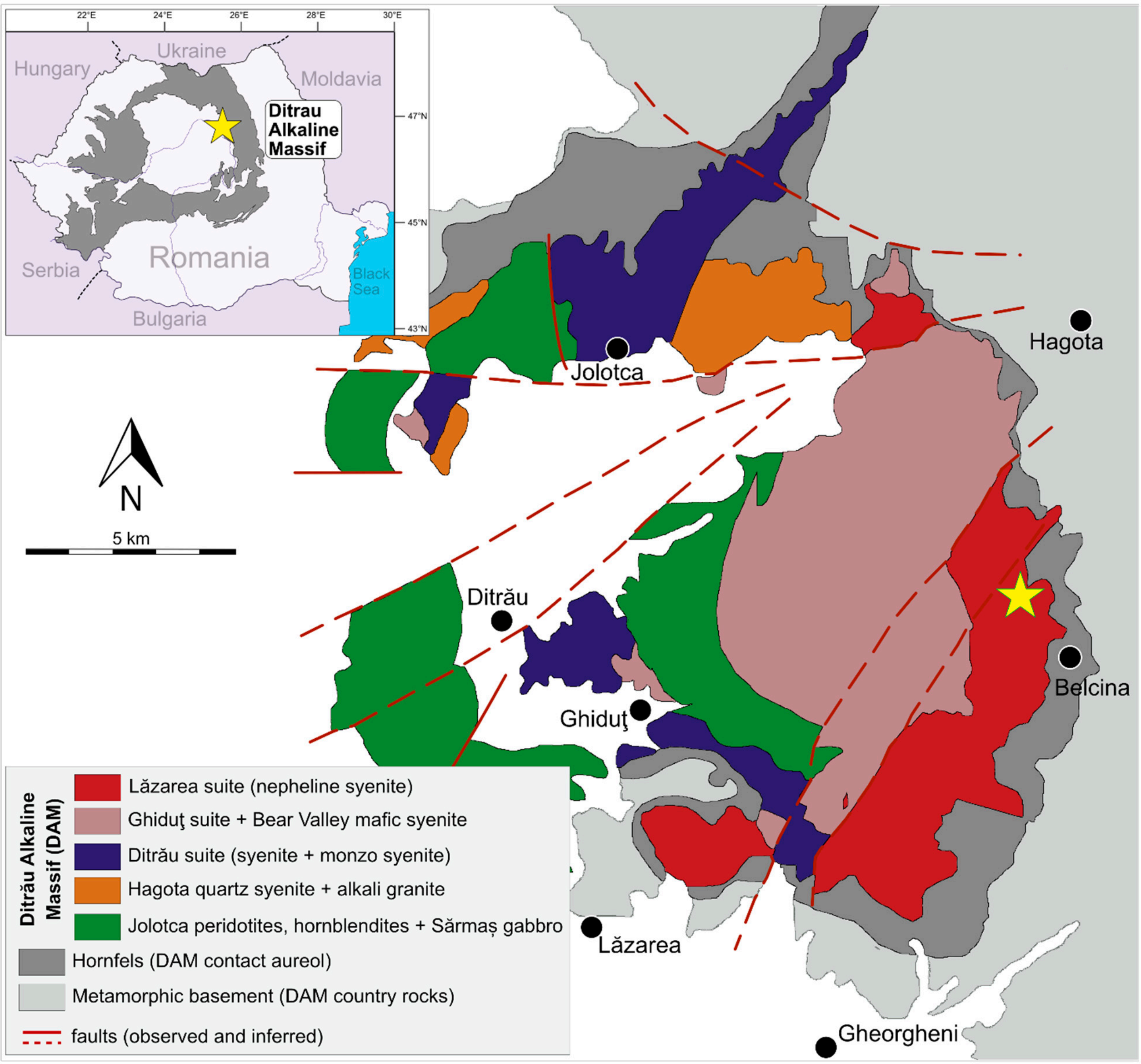

Figure 1. Geological map of the Ditrău Alkaline Massif (DAM) after [17,18]. The location of samples Ditrău 1 (Lăzarea suite) and Ditrău 2 (Ghiduţ suite) are indicated by the yellow star. The inset shows the position of the Ditrău Alkaline Massif within the Eastern Carpathians of Romania.

The DAM shows a roughly concentric setup (Figure 1) and has been described as forming a ring structure [19,20] with successively younger intrusions becoming more felsic from west to east [21,22]. More modern models propose that the at present horizontal magmatic sequence was originally vertical in orientation and subsequently tilted by nappe formation during the Alpine orogeny [22,23].

The petrography and petrology of the DAM rocks have extensively been described [16–19,21–28]. The following main lithologies can be distinguished (Figure 1): (1) In the western and northern part of the DAM mafic–ultramafic cumulate rocks ranging from peridotites, pyroxenites, and hornblendites (Jolotca hornblendites [17,22]) to alkali gabbros (Sărmaș gabbro [17]) and alkali diorites (Bear Valley mafic syenite [21]) occur. (2) Quartz syenites and alkali granites are found in the Jolotca area and the north-eastern DAM (Hagota quartz syenite [17]). On the basis of gravity and magnetic surveys, these rocks are believed to extend laterally eastward beneath the massif [25]. (3) In the center of the massif a zone of magma, mingling and igneous brecciation is found that includes gabbroic, dioritic, and syenitic lithologies. This zone was originally described as "ditró essexites" [24] and was later termed "hybrid zone" [17]. (4) East of a line Jolotca-Ditrău-Lăzarea-Gheorgheni the DAM is dominated by three alkaline intrusive suites (Figure 1):

- Ditrău suite, comprising syenites to monzo-syenites (equivalent to the "Ditrău syenite" of [17]);
- Ghiduţ suite, comprising nepheline syenites, subordinate syenites, and monzo-syenites (equivalent to the former "ditroite" and the "white nepheline syenite" [21,25,29] and the "Ghiduţ nepheline syenite" [17]);
- Lăzarea suite, comprising weakly to very strongly altered nepheline syenites (formerly "red syenite" [25] or "red, hydrothermally altered variety" [21]).

All lithological units have been significantly modified by sub-solidus interaction with late-stage magmatic fluids and are cut by secondary mafic dykes [23,28,30]. This hydrothermal system is thought to have developed within the DAM magma chamber during crystallization [17,29], causing widespread alteration of the nepheline syenites by an Na-rich fluid, and the replacement of nepheline by cancrinite and sodalite [17,21,23,25]. The mafic dykes allowed the upward migration of late-stage K-rich fluids, these thereby leaching REE (rare earth elements) and HFSE (high field strength elements) from the Ghiduţ suite [17,23,27].

The DAM is surrounded by a thermal contact aureole (labelled as "hornfelses" in Figure 1) which developed in the low-grade Tulgheş Nappe and is characterized by biotite, cordierite, andalusite, corundum, rarely spinel and alkali amphibole, and occasional chloritoid hornfels found at the immediate contact. These are followed by spotted and knotted schists more distant from the contact [31].

Furthermore, in carbonate-rich veins that crosscut the complex in the north-western DAM (Jolotca region) and the Tulgheş Nappe country rocks in the Belcina region, a REE-HFSE mineralization is hosted [17,32,33].

Crosscutting field relations suggest the following igneous evolution [6,16,20,21]:

(1) The intrusion of basic to intermediate magmas (Jolotca hornblendites s.l., Sărmaș gabbro) marks the oldest igneous event, followed by (2) the intrusion of syenitic magmas (Hagota quartz syenite and Ditrău suite) and later alkali granites. (3) Mostly undersaturated, nepheline-bearing melts (Ghiduţ and Lăzarea suites) form the youngest intrusions. This event is accompanied by hydrothermal fluids which produced widespread metasomatic alterations, especially in the syenitic complexes. (4) The magmatic activity in the DAM is terminated by the formation of nepheline syenitic dikes, aplites, pegmatites, and lamprophyres. Evidently the DAM rocks were not formed by a simple, single-step igneous fractionation process. Rather, a geochemical evolution combining a number of magma sources, mixing, and fractionation events has to be sought [23,28]. Because of these complexities, no consensus on the evolution of the DAM has been reached so far, and a number of genetic models have been published:

- Metasomatism by an Na-rich fluid [34].
- Magmatic differentiation of an alkaline magma [20].
- Partial melting of silica-poor crustal rocks producing both a basic and a sialic alkaline magma [18].
- Two geological events (intrusions) in the Upper Triassic–Lower Jurassic and in the Middle Jurassic–Lower Cretaceous. These events partly coincide with each other, suggesting that the Bear Valley mafic diorites were probably formed by hybridization of hornblendites and syenites during the second event [35].
- A complex four-stage evolution resulting in an emplacement period of the DAM of ca. 70 m.y. during the Triassic and Jurassic [36].
- Two major magma sources as well as distinct magma evolution trends were reported as the result of a study of the major and trace element composition of clinopyroxenes [28]. Accordingly, a primitive diopside population is derived from a camptonitic magma (termed "Magma1") which is related to basanitic parental melts [30], whilst diopside–hedenbergite crystals represent a more Na-, Nb-, and Zr-rich magma source (termed "Magma2" and recognized for the first time in the Ditrău magmatic sys-

tem). This "Magma2" fractionated towards ijolitic (termed "Magma2a") and later phonolite (termed "Magma2b") compositions. Field observations, petrography, and clinopyroxene-melt equilibrium calculations reveal magma recharge and mingling, pyroxene recycling, fractional crystallization, and accumulation. Repeated recharge events of the two principal magmas ("Magma1", "Magma2") resulted in multiple interactions, such as magma mixing, between more primitive and more fractionated coexisting magma batches. Magma mingling also occurred between mafic and felsic magmas by injection of ijolitic magma into dikes with a phonolitic melt.

- The importance of the hydrothermal system that developed within the DAM magma chamber during crystallization was emphasized by [17]. Geochemical and petrological data from the alkaline igneous rocks, dykes, and veins within the DAM reveal the interplay of magmatic processes with late-stage magmatic and hydrothermal fluids. A hydrothermal system developed within the DAM magma chamber during the later stages of magmatic crystallization, causing localized alteration of nepheline syenites by an Na-rich fluid. Mafic dykes subsequently acted as conduits for late-stage, more K-rich fluids, which leached REE and HFSE from the surrounding syenitic rocks. These fluids percolated up and accumulated in the roof zone, causing the breakdown of nepheline to K-rich pseudomorphs and the precipitation of hydrothermal minerals such as zircon and pyrochlore within veins. The DAM and country rocks were subsequently cut by REE-mineral-bearing carbonate-rich veins. Monazite and xenotime are the main REE-bearing phases in these veins, crystallizing from a late REE- and carbonate-rich fluid with pH-controlled REE deposition.
- A dominant mantle origin of hornblendites, diorites, and nepheline syenites follows from an isotope geochemical study [23] showing age-corrected ε_{Nd} values that range from + 0.8 to + 5.5‰. High-temperature equilibrium O-isotope fractionations between minerals are thereby generally preserved, although some sub-solidus O-isotope re-equilibration occurred. Magma $\delta^{18}O$ values estimated from quartz, feldspar, and amphibole (5.7–11.7‰) are higher than those estimated from zircon. This is attributed to continuous crustal contamination, with zircon recording the early, high-temperature $\delta^{18}O$ values, and quartz and the other silicate $\delta^{18}O$ values reflecting a combination of subsequent crustal contamination and deuteric alteration. Negative correlations between calculated magma $\delta^{18}O$ values and Na_2O and Al_2O_3 content and εNd are consistent with the suite of felsic rocks from nepheline syenite to granite, resulting from an increased crustal input. The Nd- and O-isotope composition of the silica-oversaturated rocks can be explained by the assimilation of 20–60% upper crustal melts into re-injected mafic alkaline parent magma.

2.2. Former Geochronological Investigations

In the following, a short delineation of the published absolute age data on DAM rocks is given. An extensive list of published radiometric age data can be found in [6]. The first published radiometric age data from DAM rocks are from [37]. Using a total U-Th-Pb method, zircons and monazites were dated at 297 Ma and 326 Ma, respectively, the authors therefore implying a Variscan emplacement of the DAM. On the other hand, published K/Ar DAM whole-rock dates range from 196 ± 6 Ma to 121 ± 2 Ma [38], suggesting that the red nepheline syenites are older than the syenites and white nepheline syenites, which are supposed to be of the same age. Biotite and whole-rock K/Ar cooling dates from nepheline syenites, hornfelses, and tinguaite dikes ranging from 161 ± 7 Ma to 150 ± 6 Ma were presented by [20]. The authors state that the slightly older whole-rock age of the tinguaite dikes is probably nearer to the real time of emplacement, i.e., an intrusion older than Jurassic is most unlikely and an emplacement around 160 Ma seems reasonable. More K/Ar biotite, nepheline, and whole-rock dates from various lithologies ranging from 172.0 ± 6.6 Ma to 81.3 ± 3.1 Ma without any systematic relations were published by [39]. A total of 25 whole-rock K/Ar dates ranging from the Middle Triassic (hornblendite; 237.4 ± 9.1 Ma) to the Lower Cretaceous (alkaline feldspar syenite; 107.6 ± 4.1 Ma) were published by [35]. These data were interpreted as indicating two individual intrusion events. Multigrain hornblende concentrates from two samples of a massive gabbro and a diorite from "early" DAM intrusive phases (i.e., Sărmaș gabbro) recorded $^{39}Ar/^{40}Ar$ plateau ages of 231.5 ± 0.1 Ma and 227.1 ± 0.1 Ma. These were interpreted as dating relatively rapid cooling at high crustal levels following pluton emplacement in the Middle–Late Triassic [40]. A zircon emplacement age by conventional multigrain U-Pb dating of 229.6 +1.7/−1.2 Ma for a medium-grained Ditrău syenite from Jolotca was reported by [31]. According to the authors, the Ladinian zircon age matches within the uncertainty the hornblende $^{36}Ar/^{40}Ar$ vs. $^{39}Ar/^{40}Ar$ dates obtained from the diorite complex [40] and hints to a relatively short magmatic evolution of the DAM. This finding is thought to validate the original interpretation of [19] and questions the speculations of a 15 m.y. time gap between the emplacement of the gabbros and Ditrău syenites, as discussed by [36]. Preliminary LA-ICP-MS U-Pb dates for titanite from amphibolites and altered roof-zone nepheline syenite indicating a magmatic age of ca. 230 Ma were presented by [27]. From the northern part of the complex near Jolotca, [6] reported amphibole and biotite K-Ar ages from a cumulitic nepheline syenite and three granite samples, respectively. The reported ages range from 238.6 ± 8.9 Ma to 196.3 ± 7.4 Ma. The same authors also report in situ U-Pb ages: titanite and zircon from syenite were dated at 225.3 ± 2.7 Ma and 232.4 ± 3.3 Ma, respectively. A nepheline syenite sample gave a U-Pb titanite age of 230.6 ± 3.5 and a zircon age of 230.6 ± 2.4 Ma. Considering the new and previous (post-1990 year) K-Ar and U-Pb data, the authors conclude that the crystallization of the DAM took place between 238.6 ± 8.9 and 225.3 ± 2.7 Ma (noting that the most relevant U-Pb ages scatter around ∼ approx. 230 Ma).

3. Materials and Methods

3.1. Microscopy and Whole-Rock Analysis

Representative samples of the nepheline syenite from the Lăzarea suite (sample Ditrău 1) and the Ghiduţ suite (sample Ditrău 2), weighting about 10 kg each, were collected in the abandoned Lăzarea suite quarry in the upper reaches of the Belcina Valley (location: yellow star on Figure 1; 46°48′51.2″ N/25°40′7.7″ E) in the easternmost part of the DAM.

3.2. Microscopy and Whole-Rock Analysis

Petrographical observations were used to select representative samples for whole-rock geochemical and isotopic investigations as well as for U-Pb zircon dating. Whole-rock analyses were undertaken by X-ray fluorescence (XRF) for major and large ion lithophile trace elements (LILE) and by inductively coupled plasma mass spectrometry (ICP-MS) for high field strength elements (HFSE) and rare earth elements (REE) at the Bureau Veritas (Canada). Preparation involved lithium borate fusion and dilute digestions or hot four-acid digestion for ICP-MS, $LiBO_2$ fusion for XRF, and lithium borate decomposition or aqua Regia digestion for ICP-MS. Loss of ignition (LoI) was determined at 1000 °C. Uncertainties for the major elements are 1%, except for SiO_2, which is 0.1%. REEs are normalized to C1 chondrite.

3.3. Zircon Separation and Cathodoluminescence (CL) Imaging

Zircon crystals were separated using standard density separation techniques (crushing, sieving, Wilfley table, heavy liquid, and magnetic separation) at the Laboratory of Lithospheric Research, University of Vienna (Austria). Zircon grains were handpicked under a binocular microscope and mounted on standard 1-inch epoxy resin discs together with chips of zircon reference material Temora 2 and Plešovice, then ground and polished to approximately half their thickness to expose internal structures.

The chemical zonation of the zircon crystals was revealed by cathodoluminescence (CL) imaging using an FET Philips 30 electron microscope (accelerating voltage of 15 kV with a beam current of 20 nA) at the Institute of Earth Sciences, University of Silesia in Katowice (Poland). The most suitable locations for in situ U-Pb dating were selected according to zonation patterns and degree of alteration. Zircon grains were again imaged after the SIMS analyses in order to define the precise spot location with respect to internal micro-structures.

3.4. SIMS U-Pb Dating

Zircon U-Pb SIMS analyses were conducted using a CAMECA IMS-1280 HR instrument at the Institute of Geology and Geophysics, Chinese Academy of Sciences (Beijing, China), during one session. A hybrid dynamic multi-collector U-Pb dating technique was used, taking advantage of both the static multi-collector mode and peak-hopping mono-collector mode and using oxygen flooding. The instrument description and analytical procedure are given in [41,42]. Final age data reduction was carried out using the offline version of IsoplotR [43]. Uncertainties on individual analyses in Table 2 are reported at the 1 RSD (relative standard deviation) level, whereas final U-Pb ages are quoted with 2 SD confidence intervals and with decay constant uncertainties included.

4. Results

4.1. Petrography

4.1.1. Lăzarea Suite (Sample Ditrău 1)

The Lăzarea suite sample (previously named “red syenite” [16] or “red, hydrothermally altered variety” [21]) is a reddish, variable from medium- to coarse-grained massive rock (Figure 2). It is characterized by centimeter-sized alkali feldspars, dull green micaceous pseudomorphs after nepheline (liebnerite; [18]), and up to 15 vol% biotite and amphibole, each. The proportion of mafic minerals decreases to 5% as grain size increases. They typically form mafic accumulations, a few millimeters across, and commonly contain apatite, titanite, sulfide, zircon, epidote group, and carbonate minerals (Figure 2, [21]). Zircons, generally < 0.4 mm in diameter, occur interstitially, but are also found in fractures that are up to 1 mm wide and also host monazite, allanite, bastnaesite, pyrochlore, and magnetite. Overall, HFSE-bearing accessory minerals are more abundant in the Lăzarea suite than in other lithologies [21,27].

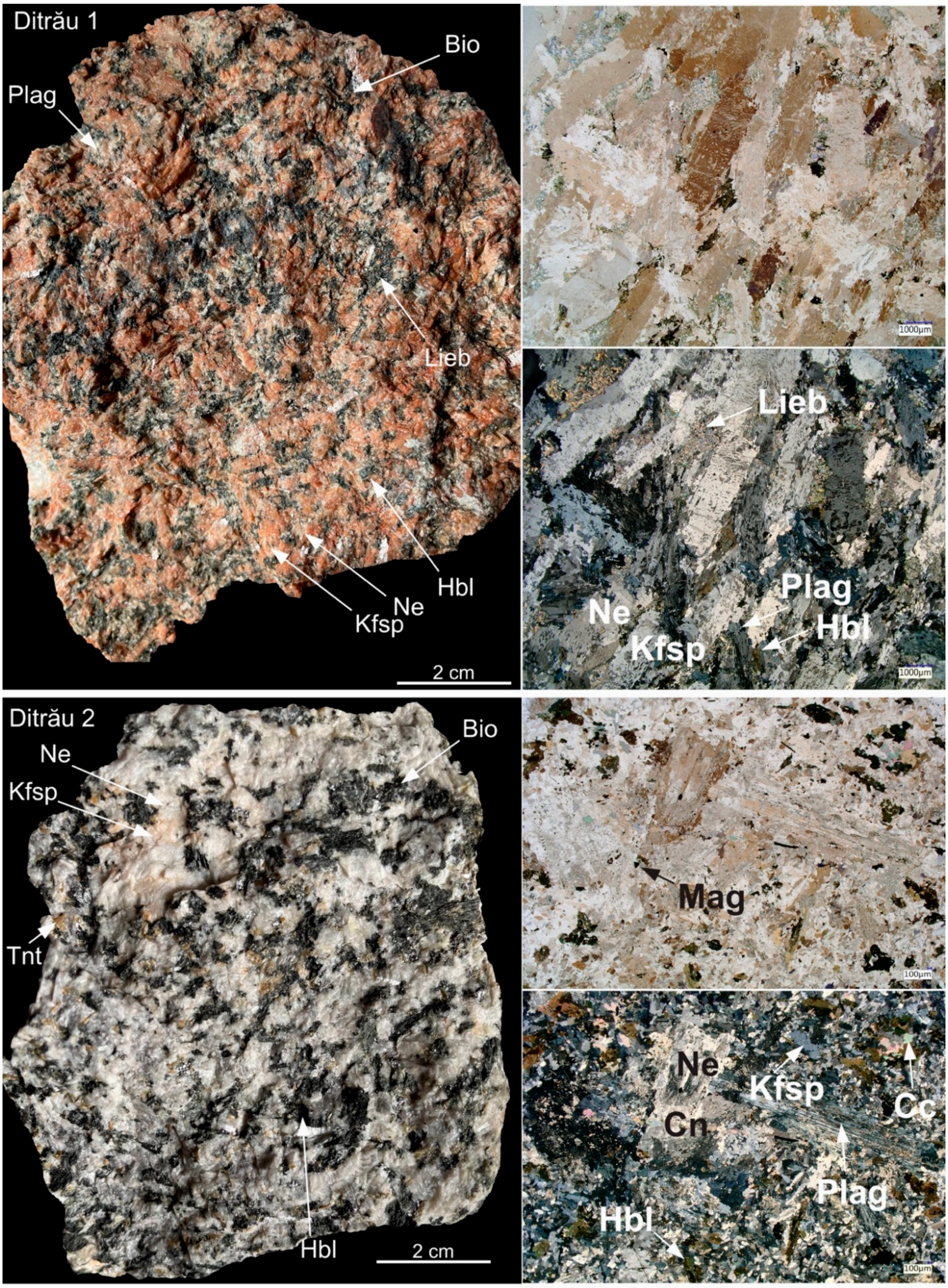

Figure 2. Macro- and microphotographs of the investigated samples from the DAM. (Ditrău 1) Hand specimen of the Lăzarea suite nepheline syenite and thin section images. Upper image in plane polarized light, lower image in double polarized light. (Ditrău 2) Hand specimen of the Ghiduţ suite nepheline syenite and thin section images. Upper image in plane polarized light, lower image in double polarized light. In all images the major mineral phases are labelled; Bio = biotite, Cc = calcite, Cn = cancrinite, Hbl = hornblende, Kfsp = potassium feldspar, Lieb = liebernite, Mag = magnetite, Ne = nepheline, Plag = plagioclase, Tnt = titanite.

4.1.2. Ghiduţ Suite (Sample Ditrău 2)

The Ghiduţ suite sample is a light gray, medium- to coarse-grained massive rock (Figure 2). The sample is characterized by medium-grained, often tabular alkali feldspar (orthoclase, microcline, and perthite) and large euhedral nepheline (up to 1 cm) set in a finer-grained alkali feldspar-rich groundmass. The alkali feldspars have undulous grain boundaries and no preferred orientation. Plagioclase, found only in the groundmass, comprises up to 10 vol% of the rock. Aegirine, amphibole, muscovite, and biotite are present (max. 20 vol%) in medium-grained nepheline syenites, but not in the coarsest varieties. Accessory minerals are titanite, zircon, monazite, pyrite, pyrochlore, thorite, zirconolite, molybdenite, magnetite, ilmenite (often characteristically skeletal), and rutile. Ultramafic enclaves up to a few centimeters in size are locally present. They are dominated by pyroxene, amphibole, and biotite, with < 10 vol% leucocratic minerals [21].

In the Ghiduţ suite alteration of nepheline is variable and can be separated into two distinct types [17,29]. The first is the alteration of nepheline to cancrinite (Figure 2). Between cancrinite crystals, sodalite, muscovite, pyrochlore, magnetite, and ilmenite occur. The second alteration phase shows fine-grained muscovite aggregates replacing nepheline and cancrinite. The two types of alteration can coexist within a single nepheline grain, with muscovite alteration more common in the core and cancrinite more common along the grain boundaries. Alteration textures around aegirine are also common [28]. The most altered samples contain large biotites where all nepheline has been altered to micaceous aggregates and/or cancrinite, similar to textures present in the Lăzarea suite (see below).

4.2. Whole-Rock Chemistry

Major, trace, and rare earth element data for the two samples are reported in Table 1 and shown in Figure 3. According to the major element composition (SiO_2 versus Na_2O + K_2O [44]), sample Ditrău 1 is a syenite (blue dot on Figure 3a), whereas sample Ditrău 2 is a nepheline syenite (green dot on Figure 3a). Both samples are slightly peraluminous (ASI = 1.12 and 1.01) and strongly peralkaline (AI = 1.56 and 1.63). Ditrău 1 has high Na_2O and K_2O concentrations of 6.32 wt.% and 6.37 wt.% at 62.5 wt.% SiO_2. Ditrău 2 has also high Na_2O and K_2O concentrations of 9.22 wt.% and 4.43 wt.% at 57.7 wt.% SiO_2. CaO in both samples is low (0.19 wt.% and 1.12 wt.%), as is Fe, Mg, and Mn (Table 1). In the TAS (total alkalies versus silica) discrimination diagram [45], the samples plot within the delineated compositional fields of the published data from the Ghiduţ and Lăzarea suites, respectively [17,23,26].

Table 1. Whole-rock geochemistry data.

	Major elements (weight-%)							
	SiO_2	TiO_2	Al_2O_3	$Fe_2O_{3\,tot}$	MnO	MgO	CaO	Na_2O
Ditrău 1	62.5	0.18	19.8	1.66	0.04	0.16	0.19	6.32
Ditrău 2	57.7	0.25	22.2	2.05	0.05	0.22	1.12	9.22
	K_2O	P_2O_5	LOI	Total	ASI	alkalinity		
Ditrău 1	6.37	0.03	1.44	98.7	1.12	1.561		
Ditrău 2	4.43	0.04	0.94	98.2	1.01	1.627		
	Trace elements (µg/g)							
	Cs	Rb	Ba	Th	U	Ta	Nb	Mo
Ditrău 1	0.5	262.8	306.8	15	8.5	4.1	248.3	7.4
Ditrău 2	0.7	149.3	1053.7	29.3	12.5	8.2	222.4	0.6
	La	Ce	Sr	Nd	Hf	Zr	Y	
Ditrău 1	26.7	36.4	111.7	7.5	18.6	1214.1	8.5	
Ditrău 2	34.9	58.2	606	17	13.1	747.3	9.6	

Table 1. *Cont.*

	REE (μg/g)								
	La	Ce	Pr	Nd	Sm	Eu	Gd	Tb	
Ditrău 1	28.5	36.9	2.6	7.9	1.02	0.27	0.93	0.17	
Ditrău 2	33.5	57.3	5.1	16.8	2.31	0.79	1.98	0.28	
	Dy	Ho	Er	Tm	Yb	Lu	Total	La/Sm	Gd/Yb
Ditrău 1	1.18	0.28	0.96	0.2	1.67	0.28	78.2	17.5	0.5
Ditrău 2	1.66	0.36	1.1	0.19	1.13	0.21	118	9.1	1.4
	Zr saturation temperatures (°C)								
	Zr	G *	B **	model Zr	G *	B **	model Zr	G *	B **
Ditrău 1	1214	1007	971	900	953	927	400	808	821
	uncertainty ***	18	18		18	18		18	18
Ditrău 2	747	865	846	620	832	824	400	754	774
	uncertainty ***	18	18		18	18		18	18

* = Gervasoni et al. (2016) [46], ** = Boehnke et al. (2013) [47], *** = All uncertainty estimates are based on an uncertainty of 10% on the Zr concentration.

Total REE concentrations are 82.8 μg/g (Ditrău 1) and 122.7 μg/g (Ditrău 2). On the chondrite-normalized diagrams [48] both samples show steep, sub-parallel trends, strong LREE enrichment with (La/Sm)N = 17.5 and 9.1, flat HREE (heavy rare earth elements) patterns with (Gd/Yb)N = 0.5 and 1.4, and plot into the fields defined by literature REE data (Figure 3b [17,21,23]). In detail, Ditrău 1 (thick gray line on Figure 3b) follows a trend intermediate between the mean Lăzarea suite composition and the most altered and enriched sample (dashed blue line on Figure 3, sample DD24, [17]). Ditrău 2 (thick gray line on Figure 3b) very closely corresponds to the mean Ghiduţ suite composition of [17]. On the trace element spider plots normalized to the average upper crust [48], again both samples plot within the designated fields of published data but Ditrău 1 shows an extreme enrichment of Rb, Nb, Zr, Hf, and, contrariwise, depletion of Cs and Ba (thick gray line on Figure 3c). Ditrău 2, on the other hand, follows the common trace element trend of the literature data at the higher concentration ranges (thick gray line on Figure 3c).

Zirconium saturation temperatures using the measured Zr concentrations of 1214 μg/g for Ditrău 1 and 747 μg/g for Ditrău 2 and the calibration of [46] are 1007 °C and 865 °C, respectively. Somewhat lower temperatures (by 20–40 °C) are returned by the [47] calibration, resulting in 971 °C and 846 °C (Table 1). A whole-rock Zr-Hf correlation diagram of all DAM syenite data is shown on Figure 4. Most samples plot on a statistically well-defined reference line (red dashed line), indicating a common whole-rock Zr/Hf ratio of ca. 50 for the various DAM syenites. In contrast, a number of Lăzarea suite samples including the sample Ditrău 1, and to a lesser degree, the sample Ditrău 2, deviate markedly from this primary reference line to higher Zr concentrations, and probably also somewhat higher Hf concentrations (see also Figure 3c). This secondary reference line indicates the addition of Zr and Hf to the altered samples with a Zr/Hf ratio of ca. 80. Assuming mostly Zr and far lesser Hf gain, projection of the Ditrău 1 and Ditrău 2 Zr concentrations onto the primary Zr/Hf = 50 reference line (dashed arrows on Figure 4) leads to model Zr concentrations of ca. 900 μg/g and ca. 620 μg/g for these two samples, respectively. The resulting [46] Zr saturation temperatures are then 953 °C and 832 °C. The intersection of the primary and secondary reference lines results in Zr and Hf concentrations of ca. 400 μg/g and 8.5 μg/g, respectively (Figure 4).

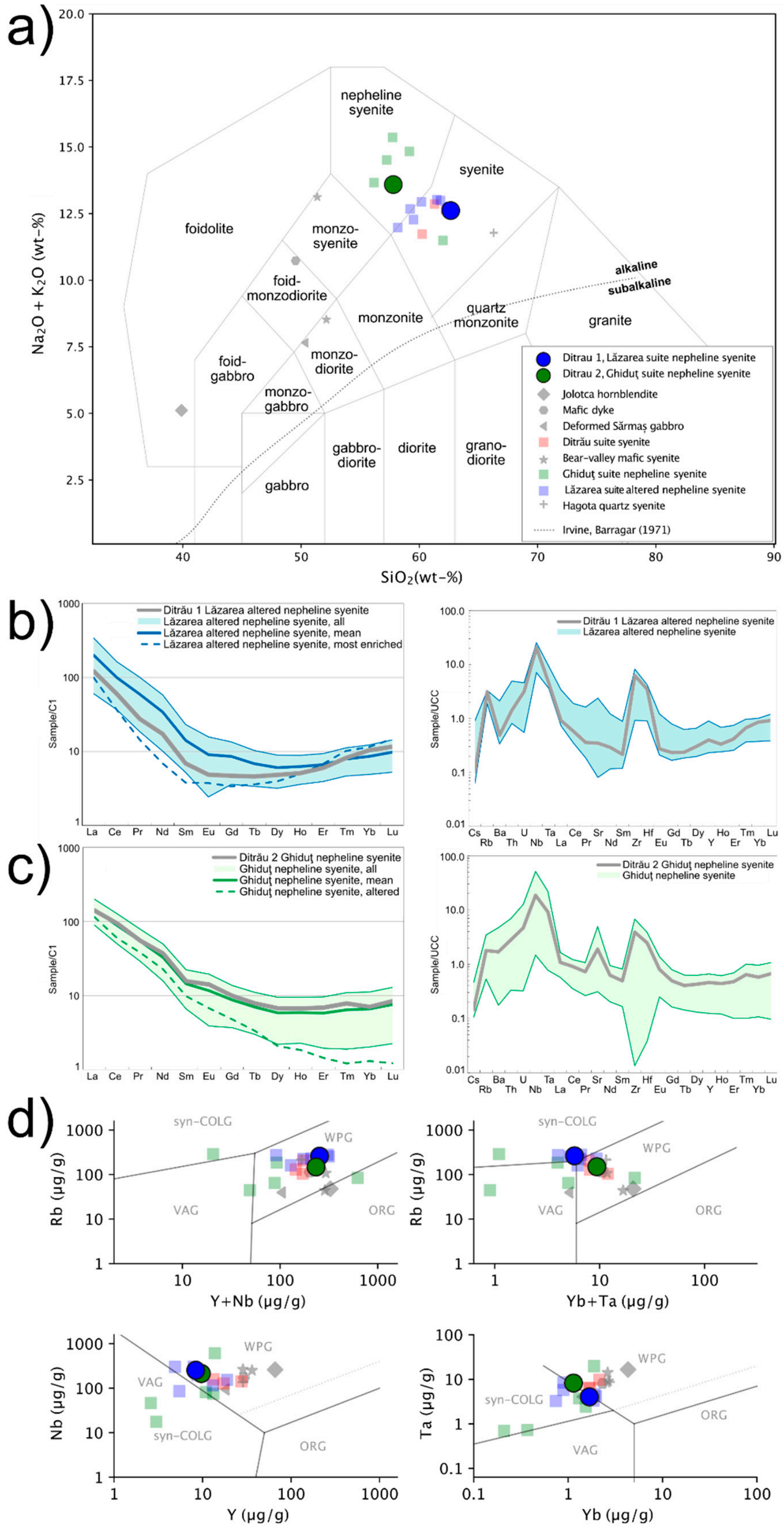

Figure 3. Geochemistry plots. The data are given in Table 1. (**a**) TAS classification after [45]. Blue dot: Ditrău 1, Lăzarea suite nepheline syenite; green dot: Ditrău 2, Ghiduţ suite nepheline syenite. Literature data shown in light shading are from [17]. (**b**) Chondrite-normalized REE concentrations using the values of [48]. Blue field: literature data of the Lăzarea suite; green field: literature data of the Ghiduţ suite. The respective thick gray lines are the data from this study. Literature data are from [17] and [23]. (**c**) Trace element spider diagrams with values normalized to the average upper continental crust of [48]. Blue field: literature data of the Lăzarea suite; green field: literature data

of the Ghiduţ suite. The respective thick gray lines are the data from this study. Literature data are from [17]. (**d**) Tectonic discrimination diagrams after [49]. Blue dot: Ditrău 1, Lăzarea suite nepheline syenite; green dot: Ditrău 2, Ghiduţ suite nepheline syenite. Literature data shown in light shading are from [17]. Symbols are as in subfigure (**a**).

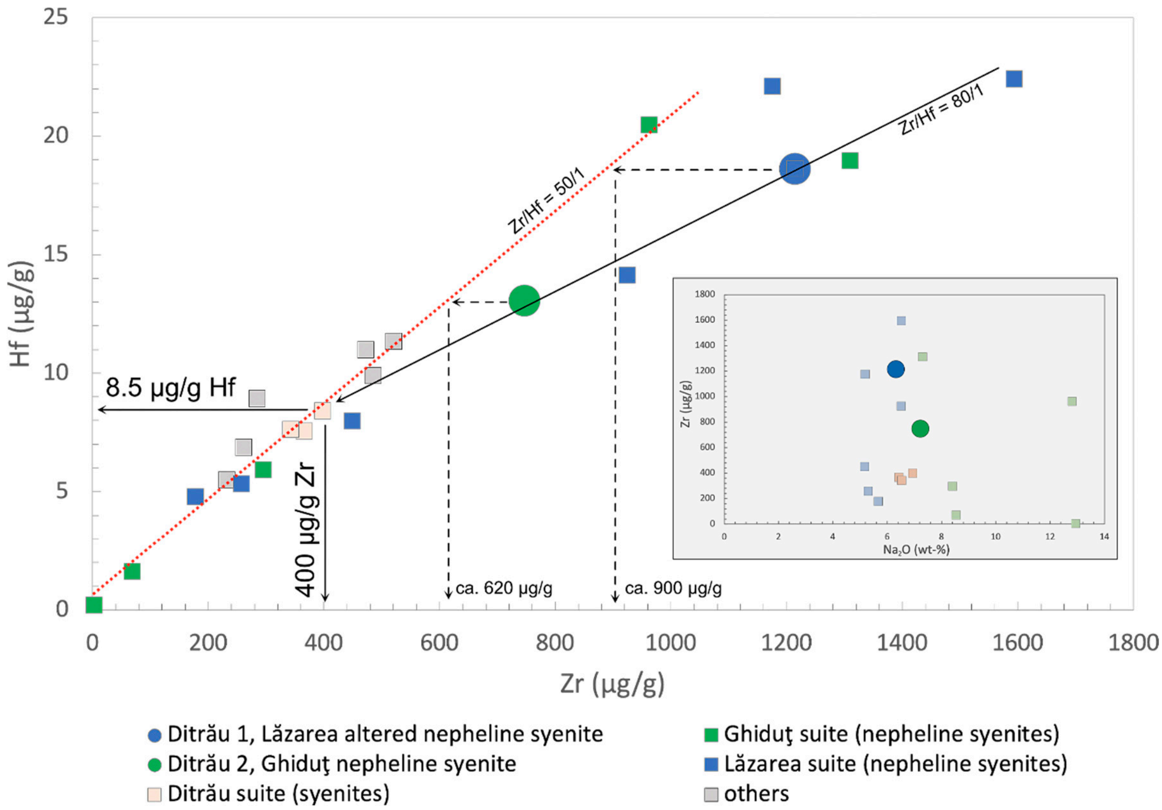

Figure 4. Zr-Hf whole-rock systematics of the DAM intrusives. The red dashed line refers to the average Zr/Hf ratio of the DAM syenites and nepheline syenites showing different degrees of metasomatic/hydrothermal alteration. The two samples Ditrău 1 and 2 evidently lie off this reference line, indicating a metasomatic/hydrothermal agent relatively enriched in Zr, resulting in a model Zr/Hf ratio of ca. 80 (black arrow). The dashed and full black arrows indicate endmember Zr and Hf concentrations derived from different petrogenetic models. The inset shows the Na_2O versus Zr systematics of the DAM alkaline rocks, demonstrating that there is no correlation of Na_2O with Zr. See text for further discussion. Symbols are as in Figure 3a with the exception of "others" which designates literature data from hornblendites, the Sărmaș gabbro, the Bear Valley mafic syenite, and the Hagota quartz syenite. Literature data are from [17,23].

The analyzed samples together with the literature data [17,23,26] suggest an origin from a within-plate environment with a slight tendency towards syn-collisional geochemical signatures on the granite discrimination diagram [48] (Figure 3d).

4.3. Zircon Characteristics

Ditrău 1: Zircon crystals are hypidiomorphic to xenomorphic, 50 µm to 500 µm in size. Crystals are colorless to pinkish and clear to turbid. In the colorless zircons, thorite inclusions are spread throughout the crystals, whereas titanite, apatite, zoisite/clinozoisite, and Ca-rich unidentified inclusions are concentrated in the rims.

CL images reveal different chemical zonation patterns and that the grains are partly broken fragments of originally bigger crystals. Around 20% of the crystals are dominated by a crystallographically oriented, CL-bright to relatively CL-dark, fine- to coarse-scaled oscillatory zonation, typical for crystal growth from a melt (Figure 5; e.g., crystals 6, 7, 12a, 25b). Some crystals show CL-bright, featureless small recrystallization internal domains and/or rims (Figure 5; e.g., crystals 6, 11, 19). All these zircons are xenomorphic to hypidiomorphic and do not show any significant inclusions.

The remaining ca. 80% of the zircons show very complex internal zonation features, some definitely characteristic for replacement of a former igneous zircon (Figure 6; e.g., crystals 1, 2), others representing new growth (Figure 6; e.g., crystals 4, 5). Overprinting thereby ranges from only partial replacement of igneous zircon from the rim and/or center (Figure 6, e.g., crystals 1, 2) to complete replacement (Figure 6, e.g., crystal 3). The replacement domains are not crystallographically oriented, and are patchy, either with a bright or an intermediate CL emission. Boundaries between these two domains are mostly sharp. Very often the center domains of the crystals are filled by non-Cl-active apatite (Figure 6, e.g., crystals 4, 5). Overall, the range of the CL emission of these zircons is identical to the CL emission of the purely igneous zircons.

In contrast to the xenomorphic to hypidiomorphic igneous zircons (Figure 5), the zircon crystals thought to have grown afresh often show a stubby and idiomorphic habit (Figure 6; e.g., crystals 4, 5).

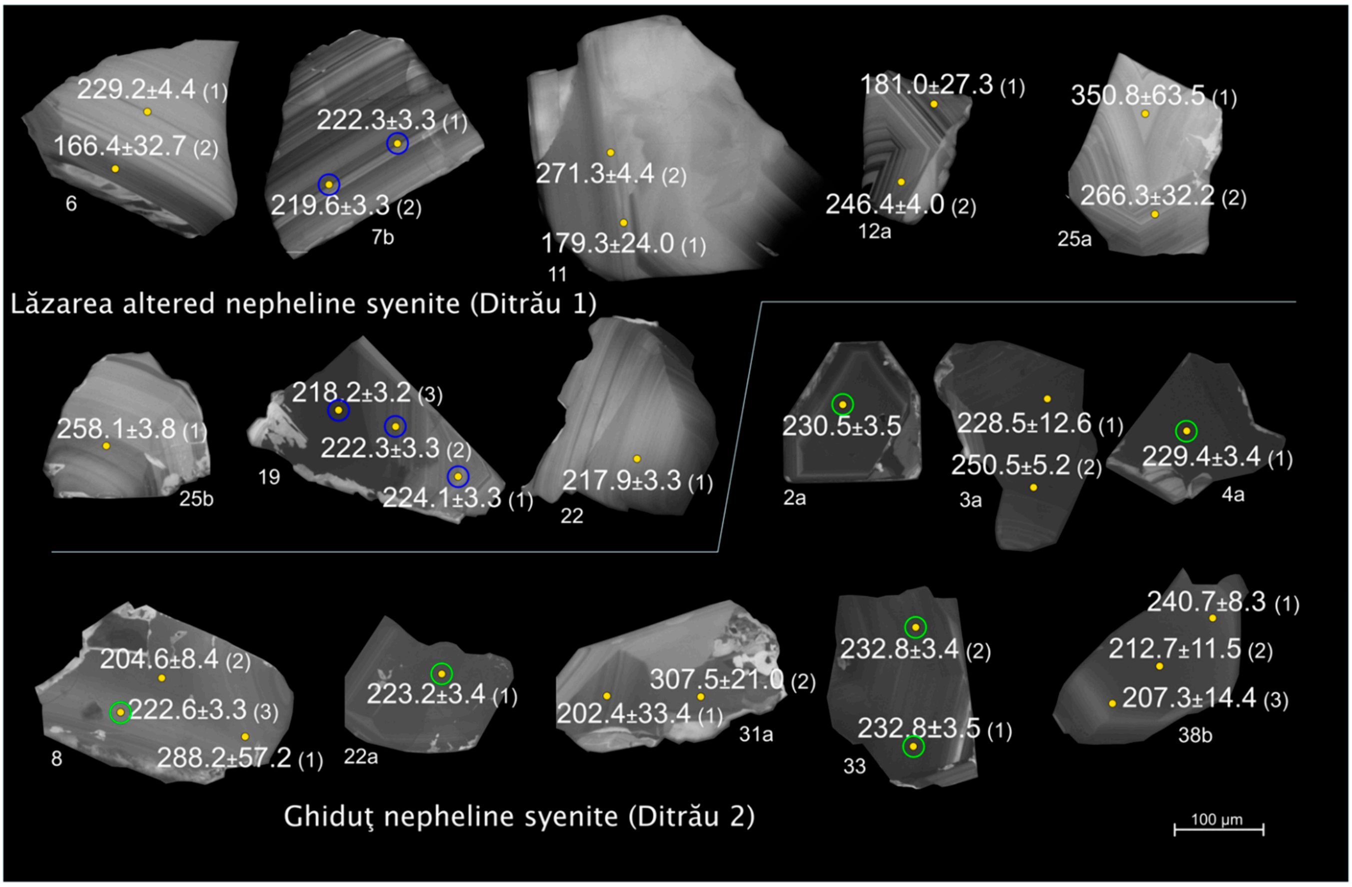

Figure 5. Zircon CL images with SIMS spots indicated as yellow dots (true size 5 × 7 µm). Zircon labels refer to the numbering in Table 2. Numbers in brackets refer to the spot numbers on the individual crystals. Ages are $^{238}U/^{206}Pb$ ages ± 2 standard deviations. The spots circled in blue ($^{238}U/^{206}Pb > 25$ and $Th/U > 15$, CL-dark domains, weakly visible oscillatory zonation) and green ($^{238}U/^{206}Pb > 25$ and $Th/U < 5$, intermediate bright CL domains, well-developed oscillatory zonation) correspond to the spots used to calculate the igneous zircon growth ages (see Figure 7).

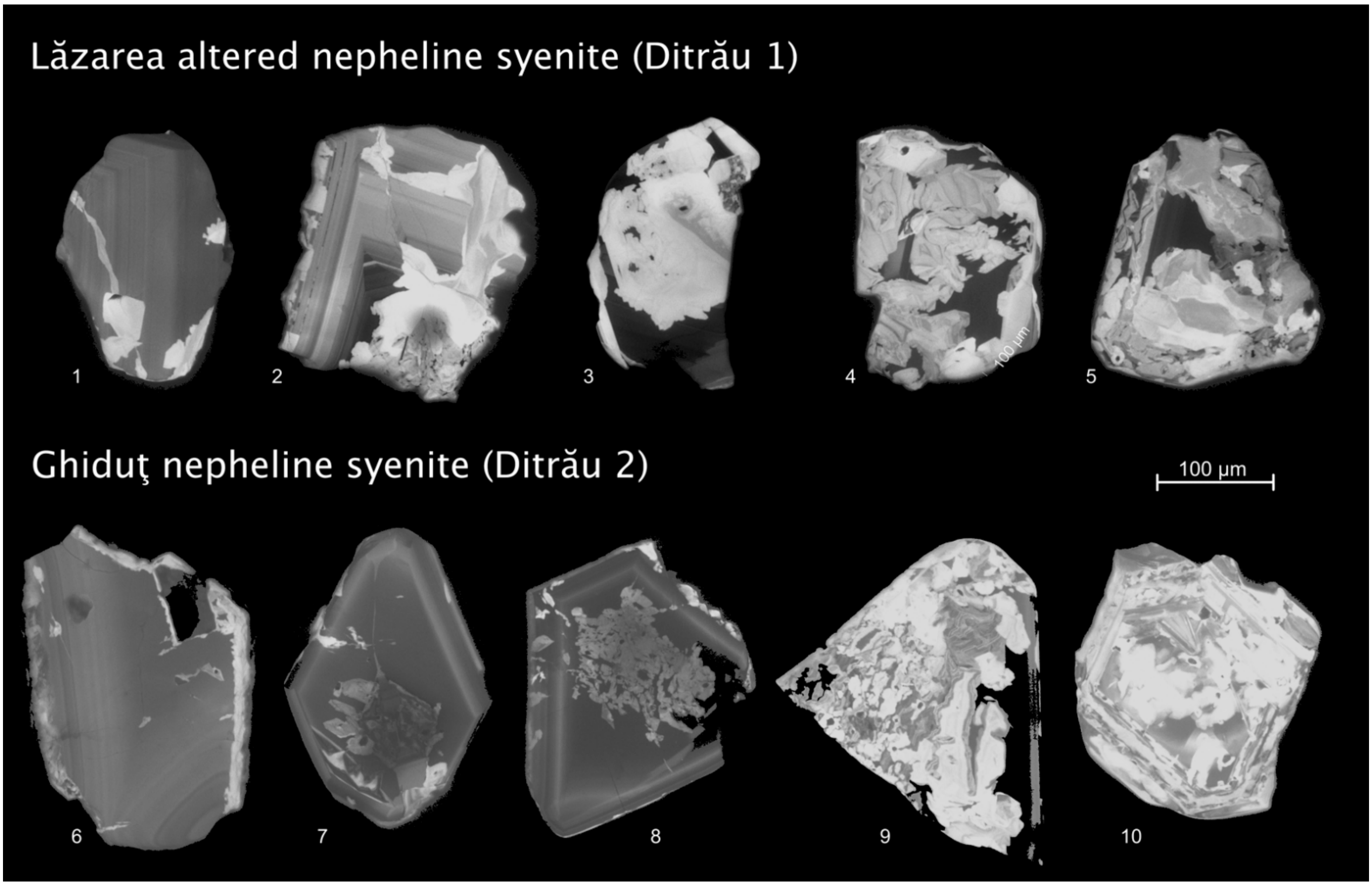

Figure 6. Zircon CL images showing crystal with a moderate (crystals 1, 6) to complete metasomatic/hydrothermal overprinting or new growth (crystals 5, 10).

Ditrău 2: Zircon crystals are idiomorphic to hypidiomorphic, up to 2 mm in diameter. Crystals are colorless and clear, mostly unfractured, often with an inclusion-free center and a heterogeneous zone with multiple inclusions of LREE, Y, Th-, and/or Nb-bearing mineral phases of varying sizes towards the rim. CL images of high-quality crystals reveal two different chemical zonation features. About half of the investigated crystals are dominated by domains with a comparably dark CL emission and a weakly visible oscillatory zonation (Figure 5; crystals 2a, 3a, 4a, 8, 22a). Some crystals show patchy, non-systematic CL-bright inner domains and rims, often associated with numerous non-CL emitting inclusions (Figure 5; crystals 8, 31a). The remaining ca. 50% of the zircons show very complex overprinting features. They are mostly patchy and CL-brighter than the former domains. Overprinting ranges from only partial replacement of igneous zircon from the rim and/or inner domain (Figure 6, e.g., crystals 6, 7, 8) to complete replacement (Figure 6, e.g., crystals 9, 10). Replacement is systematic. It starts with a zone with an intermediate CL emission in the inner domains of the crystals (Figure 6, e.g., crystals 7, 8), which then is replaced by a more CL-intensive zone (Figure 6, e.g., crystal 9). This CL-bright zone can also be found along the rims of the crystals (Figure 5, e.g., crystals 2a, 4a, 8; Figure 6, e.g., crystal 6). In contrast to the Ditrău 1, zircons replacement can be crystallographically oriented (Figure 6, e.g., crystal 10).

In general, the Ditrău 1 igneous zircons have a far brighter CL emission and better developed oscillatory zoning than the Ditrău 2 igneous zircons, whereas the CL emission intensity of the altered and/or new grown zircons are identical in the two samples (Figures 5 and 6).

Table 2. Zircon U-Th-Pb SIMS data.

	Concentrations					Atomic Ratios			
Sample/spot #	**[U] μg/g**	**[Th] μg/g**	**Th/U**	**^{206}Pb/^{204}Pb measured**	**f_{206}%**	**^{238}U */^{206}Pb**	**±1RSD %**	**^{207}Pb/^{206}Pb**	**± 1RSD %**
Ditrau1_06@1	19	223	11.8	110	16.99	22.932	2.2	0.19625	10.1
Ditrau1_06@2	5	613	129	30.1	62.04	14.517	3.8	0.47659	13.5
Ditrau1_07b@1	70	1371	19.7	225	8.31	26.134	1.9	0.10399	10.5
Ditrau1_07b@2	80	1404	17.6	207	9.04	26.244	1.7	0.09839	11.7
Ditrau1_11@1	11	212	18.9	40.6	46.11	19.104	2.1	0.34918	9.6
Ditrau1_11@2	13	192	15.0	78.1	23.95	17.691	2.6	0.25925	15.3
Ditrau1_12a@1	6	578	89.2	32.9	56.88	15.147	1.8	0.43752	10.1
Ditrau1_12a@2	22	422	19.4	86.1	21.73	20.089	2.4	0.23444	13.4
Ditrau1_19@1	140	2415	17.3	589	3.17	27.377	1.6	0.08040	6.1
Ditrau1_19@2	159	3197	20.1	454	4.12	27.324	1.6	0.08206	10.4
Ditrau1_19@3	85	724	8.5	290	6.45	27.173	1.7	0.09894	7.7
Ditrau1_22@1	49	1045	21.4	99.9	18.71	23.648	1.9	0.14787	11.4
Ditrau1_25a@1	4	472	116	44.1	42.44	10.292	12.1	0.54195	10.2
Ditrau1_25a@2	6	364	64.9	36.5	51.24	11.560	2.7	0.47464	9.6
Ditrau1_25b@1	15	381	24.8	107	17.55	20.186	2.3	0.27389	12.0
Ditrau2_02a@1	375	982	2.6	1136	1.65	27.017	1.5	0.06630	5.3
Ditrau2_03a@1	31	9507	303	67.7	27.62	20.062	2.3	0.20036	10.5
Ditrau2_03a@2	34	11,407	333	90.5	20.67	20.021	1.6	0.21139	13.2
Ditrau2_04a@1	1952	7843	4.0	4711	0.40	27.500	1.5	0.05509	2.0
Ditrau2_08@1	323	1059	3.3	86.7	21.58	17.153	19.6	0.21628	19.2
Ditrau2_08@2	19	915	47.5	51.0	36.68	19.634	2.7	0.31589	10.5
Ditrau2_08@3	275	1207	4.4	401	4.67	27.131	1.6	0.07979	8.8
Ditrau2_22a@1	182	5120	28.1	367	5.10	26.942	1.6	0.08713	7.6
Ditrau2_31a@1	8	884	115	29.9	62.48	11.764	2.0	0.56471	8.1
Ditrau2_31a@2	16	1766	113	46.9	39.84	12.311	2.9	0.36034	9.8
Ditrau2_33@1	1383	1026	0.7	2040	0.92	26.943	1.5	0.05956	3.4
Ditrau2_33@2	1752	1315	0.8	3054	0.61	27.032	1.5	0.05450	2.1
Ditrau2_38b@1	41	1206	29.1	71.9	26.00	19.447	1.5	0.28340	9.6
Ditrau2_38b@2	21	535	25.8	38.9	48.11	15.472	2.2	0.39291	9.4
Ditrau2_38b@3	19	854	44.9	40.9	45.69	16.622	2.1	0.42183	8.7

* = relative fraction of common ^{206}Pb in total ^{206}Pb in %.

4.4. SIMS U-Pb Data

Per sample, 15 spots on 8 crystals each were analyzed (Figure 5, yellow spots; Figure 7; Table 2).

Ditrău 1: The U content varies from 4.1 to 159.3 μg/g (mean: 45.5), and Th contents from 191.9 to 3196.7 μg/g (mean: 907.4). Th/U varies from 8.5 to 129.2 (mean: 39.6). ^{206}Pb/^{204}Pb varies from 30.1 to 589.4 (mean: 162.0). Apparent uncorrected spot ^{206}Pb/^{238}U ages range from 166.4 ± 32.7 Ma (spot Ditrau1_06@2) to 350.8 ± 63.5 Ma (spot Ditrau1_25a@1) with a mean of 231.5 ± 44.9 Ma. ^{207}Pb corrected ^{206}Pb/^{238}U ages range from 198.1 ± 39.4 Ma (spot Ditrau1_06@2) to 261.7 ± 20.1 Ma (spot Ditrau1_11@2) with a mean of 226.2 ± 16.2 Ma. Apparent uncorrected spot ^{207}Pb/^{206}Pb ages range from 0.0 ± 1109.0 Ma (spot Ditrau1_07b@1) to 3596 ± 535 Ma (spot Ditrau1_25a@1).

On a Tera–Wasserburg plot all data points, uncorrected for common Pb, form a well-defined linear array (Figure 7a). Calculation of a regression through all 15 data points results in a lower intercept date of 222.86 ± 4.43 Ma and ^{207}Pb/^{206}Pb = 0.795 ± 0.079 (MSWD = 0.92).

Calculating a three-dimensional discordia plane in the ^{238}U/^{206}Pb-^{207}Pb/^{206}Pb- ^{204}Pb/^{206}Pb space results in a lower intercept date of 224.91 ± 3.48 Ma (MSWD = 6.3) with an initial ^{207}Pb/^{206}Pb = 0.833 ± 0.027. Forcing the regression through ^{207}Pb/^{206}Pb = 0.851 (Stacey–Kramers model age Pb composition at 230 Ma [50]) results in a lower intercept date of 224.60 ± 3.54 Ma (MSWD = 0,98; Figure 7a). Both lower intercept dates are identical within the assigned uncertainties. For all 15 spots a strong negative correlation between $^{238}U/^{206}Pb$-$^{207}Pb/^{206}Pb$ and the Th/U ratio exists (Figure 7a, Th/U color coded ellipses). SIMS spots from zircon domains with a marked oscillatory CL zonation (Figure 5, Ditrau1_07b@1, 07b@2, 19@1, 19@2; with blue circles around yellow SIMS spots) form a tight cluster at $^{206}Pb/^{238}U > 25$ and Th/U > 15. They also show $^{206}Pb/^{204}Pb > 200$, which justifies the calculation of a concordia age after a common Pb correction (^{207}Pb correction) of the individual spots. This results in an age of 224.50 ± 3.48 Ma (MSWD = 0.2; Figure 7b).

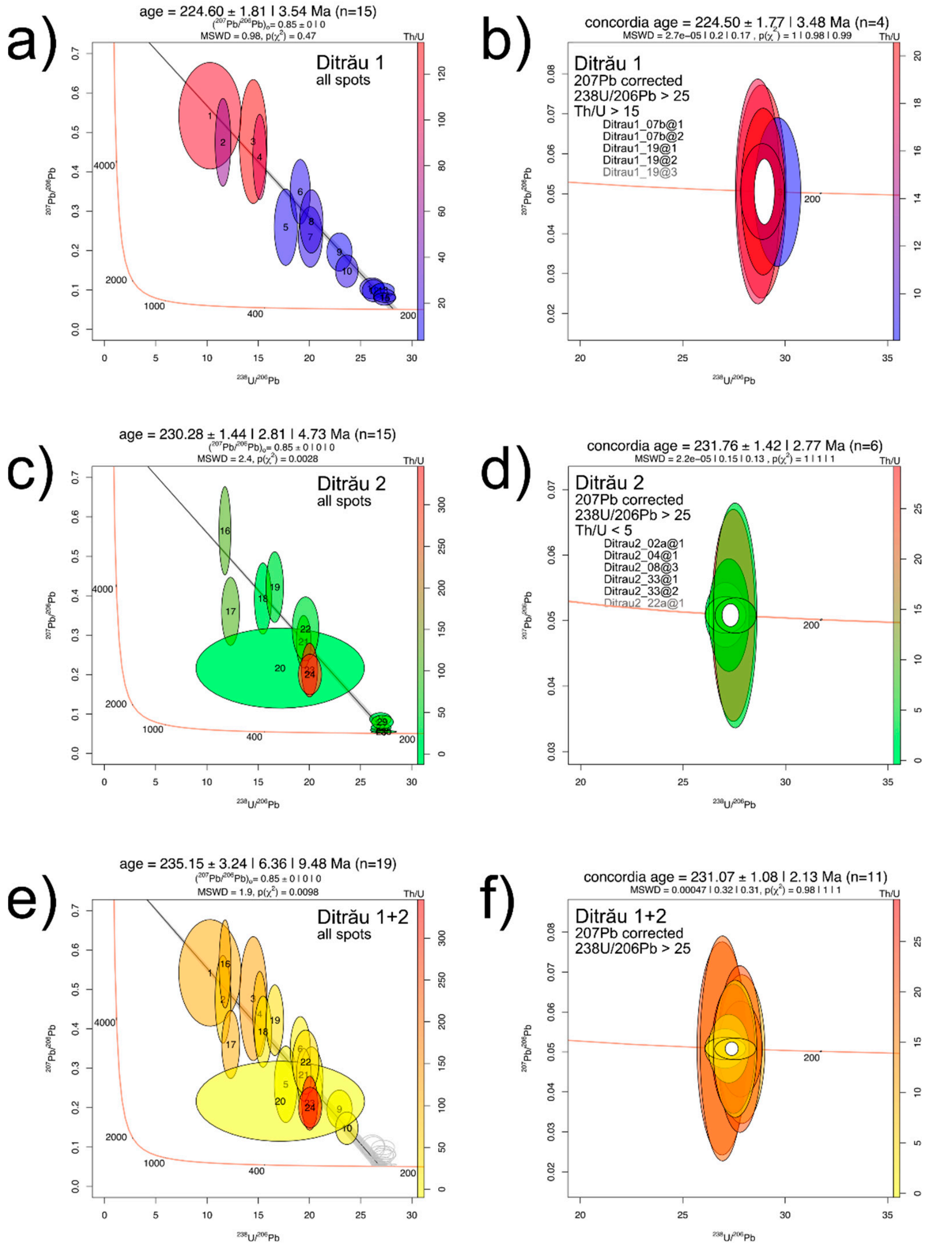

Figure 7. Zircon U-Pb Tera–Wasserburg concordia plots. (**a**) Ditrău 1 (Lăzarea suite), all data points. A forced regression through $^{207}Pb/^{206}Pb = 0.851$ results in a lower intercept age of 224.60 ± 3.54 Ma. (**b**) Ditrău 1 (Lăzarea suite), 5 data points with $^{238}U/^{206}Pb > 25$, $^{206}Pb/^{204}Pb > 200$, and ^{207}Pb corrected define a concordia age of 224.50 ± 3.48 Ma. (**c**) Ditrău 2 (Ghiduţ suite), all data points. A forced regression through $^{207}Pb/^{206}Pb = 0.851$ results in a lower intercept age of 230.28 ± 2.81 Ma. (**d**) Ditrău 2 (Ghiduţ suite), 5 data points with $^{238}U/^{206}Pb > 25$ and $^{206}Pb/^{204}Pb > 400$; (**e**,**f**) as above but combining the data from Ditrău 1 and Ditrău 2. A forced regression through $^{207}Pb/^{206}Pb = 0.851$ results in a lower intercept age of 235.15 ± 6.36 Ma. All data points with $^{238}U/^{206}Pb > 25$, $^{206}Pb/^{204}Pb > 400$, and ^{207}Pb corrected define a concordia age of 231.07 ± 2.13 Ma. See text for detailed discussion.

Ditrău 2: The U content varies from 7.7 to 1952.3 μg/g (mean: 428.9), and Th contents from 534.8 to 11,406.5 μg/g (mean: 3041.9). Th/U varies from 0.7 to 333.2 (mean: 70.4). $^{206}Pb/^{204}Pb$ varies from 29.9 to 4711.0 (mean: 815.5). Apparent uncorrected spot $^{206}Pb/^{238}U$ ages range from 202.4 ± 33.4 Ma (spot Ditrau2_31a@1) to 307.5 ± 21.0 Ma (spot Ditrau2_31a@2) with a mean of 234.2 ± 29.3 Ma. ^{207}Pb corrected $^{206}Pb/^{238}U$ ages range from 183.7 ± 38.7 Ma (spot Ditrau2_31a@1) to 308.8 ± 27.6 Ma (spot Ditrau2_31a@2) with a mean of 235.4 ± 31.4 Ma. Apparent uncorrected spot $^{207}Pb/^{206}Pb$ ages range from 0.0 ± 579.0 Ma (spot Ditrau2_08@3) to 1857 ± 1807 Ma (spot Ditrau2_31a@1).

On a Tera–Wasserburg plot all data points, uncorrected for common Pb, form a pseudo-linear array (Figure 7c). Calculation of a regression through all 15 data points results in a lower intercept date of 229.37 ± 3.03 Ma and $^{207}Pb/^{206}Pb$ = 0.793 ± 0.034 (MSWD = 2.3).

Calculating a three-dimensional discordia plane in the $^{238}U/^{206}Pb$-$^{207}Pb/^{206}Pb$-$^{204}Pb/^{206}Pb$ space results in a lower intercept date of 229.75 ± 2.83 Ma (MSWD = 3.9) with an initial $^{207}Pb/^{206}Pb$ = 0.806 ± 0.039. Forcing the regression through $^{207}Pb/^{206}Pb$ = 0.851 (Stacey–Kramers model age Pb composition at 230 Ma [50]) results in a lower intercept date of 230.28 ± 2.81 Ma (MSWD = 2.4; Figure 7c). Both lower intercept dates are identical within the assigned uncertainties. No direct correlation between $^{238}U/^{206}Pb$-$^{207}Pb/^{206}Pb$ and the Th/U ratio exists, except that individual crystals have similar intra-grain Th/U systematics (Figure 7c, Th/U color coded ellipses). SIMS spots from zircon domains with a marked oscillatory CL zonation (Figure 5, Ditrau2_02a@1, 04@1, 08@3, 33@1, 33@2; with green circles around yellow SIMS spots) form a tight cluster at $^{206}Pb/^{238}U > 25$ and $Th/U < 5$. They also show $^{206}Pb/^{204}Pb > 400$, which justifies the calculation of a concordia age after common Pb correction (^{207}Pb correction) of the individual spots. This results in a date of 231.76 ± 2.77 Ma (MSWD = 0.15; Figure 7d).

5. Discussion

5.1. Whole-Rock Geochemistry

The whole-rock geochemical data of both investigated samples show that they are representative for the nepheline syenites of the Lăzarea (Ditrău 1) and Ghiduţ (Ditrău 2) suites, respectively.

Based on the whole-rock major element data, sample Ditrău 1 can be viewed as an average Lăzarea suite nepheline syenite with only a moderate metasomatic overprinting visible in the low CaO content and only a small amount of metasomatic Na loss (see below). It very closely resembles the sample DD24 of [17], which is designated as the most enriched and most strongly mineralized Lăzarea suite sample. This is in some contradiction to the conclusions drawn from the major element geochemistry which seems to show that Ditrău 1 is only a moderately overprinted Lăzarea suite nepheline syenite. Interestingly, all samples show a common cross-over point at Er.

The whole-rock data show that Ditrău 2 is an average Ghiduţ suite nepheline syenite, albeit with a lower Na_2O content (Figure 3a).

According to the genetic model of two major magma sources [28], the so-called “Magma2” and its derivatives are characterized by pronounced HREE, Nb, Zr, and Hf enrichment accompanied by an increasing Na/Ca ratio. The TE and REE systematics of our samples and their respective petrography suggest that the Ghiduţ suite can be derived from such a “Magma2”, whereas the Lăzarea suite sample can be attributed to the phonolitic “Magma2b”, which is formed by fractionation from the parental "Magma2" [28]. In our samples, Na/Ca increases from 8.26 to 33.7 from Ditrău 2 to Ditrău 1, well in line with the observations of [28]. This geochemical sequence perfectly matches our geochronological findings, wherein the Lăzarea suite sample Ditrău 1 is significantly younger than the Ghiduţ suite Ditrău 2 sample.

5.2. Whole-Rock Zr-Hf Systematics, Zr Saturation Temperatures, and Implications for U-Pb Ages

The temperature at which Zr saturation in magmas occurs depends on the magma’s major element chemical composition and the Zr concentration [51]. In view of interpreting zircon U-Pb age data, the Zr saturation temperature denotes the temperature below which, upon magma cooling, zircon will start to crystallize. Thus, in a somewhat simplistic way, an earliest U-Pb age of a cogenetic zircon population, commonly interpreted as dating zircon growth, will date the passing of the magma through the Zr saturation temperature upon cooling.

We restrict the discussion to Zr saturation temperatures determined by the model of [46], as this takes into account all major element concentrations and therefore should deliver more realistic Zr saturation temperatures than the older, more simpler models (e.g., [47,51]). For the lithologies investigated here, the [46] temperature estimates are some 20–40 °C higher than those determined by the simpler models.

The whole-rock geochemistry of the samples Ditrău 1 and Ditrău 2 shows that Zr and Hf are strongly enriched, not only compared to normal upper crustal abundances but even to the average DAM syenites (Figure 3b,c). The enrichment process is related to a pervasive syn- to early post-magmatic overprinting event [23,28,29], and points to the derivation of the investigated rocks from an igneous source called "Magma2" [28]. According to these authors, "Magma2" is characterized by a pronounced HREE, Nb, Z, and Hf enrichment accompanied by an increasing Na/Ca ratio. Apparently, the Zr saturation temperatures of 1007 ± 18 °C and 865 ± 18 °C (Table 1) determined for these two samples are based on too high, non-equilibrium Zr concentrations, and so only can be taken as maximum Zr saturation temperatures of these two samples. Additionally, the Zr saturation temperature found for Ditrău 1 is ca. 40 °C higher than the Ditrău 2 one. In short, no decisive implications can be drawn from the Zr saturation temperatures at face value.

On the other hand, taking the Zr-Hf systematics of the alkaline DAM rocks into account, some more conclusive petrological and geochronological conclusions can be drawn (Figure 4). Evidently, two different geochemical trends can be identified. Fresh and unaltered DAM alkaline rocks lie on a well-defined trendline, indicating a common Zr/Hf whole-rock ratio of ca. 50 (Figure 4, dashed red line). Partially to completely overprinted DAM syenitic rocks, including our samples, lie below this reference line towards higher Zr/Hf ratios, indicating a more pronounced addition of Zr than Hf to the rocks by an as-yet unidentified process. An important endmember scenario can be delineated as follows: Assuming that only Zr was added to the magmatic system and that the original igneous whole-rock Zr/Hf was ca. 50, the Zr concentration of Ditrău 1 is ca. 900 µg/g and of Ditrău 2 is ca. 620 µg/g (dashed vectors on Figure 4). The equivalent Hf concentrations are then ca. 45 µg/g and ca. 31 µg/g, respectively. This means that ca. 30 wt-% of the total Zr and Hf budgets would have been added to the rocks during post-magmatic processing. As zircon is the only major Zr and Hf host in the two samples, we conclude that ca. 30% of the modal amount of zircon could be attributed to the Zr and Hf enrichment. This is an endmember scenario, as geochemically it is implausible that only Zr was added to the rocks.

The Zr-Hf data show that also the enriched rocks show a linear array, although not as well defined as the original one (Figure 4). This array shows that the rocks probably were enriched by a common agent, leading to the now observed Zr/Hf = 80 and that the original Zr and Hf contents of the rocks were more likely ca. 400 µg/g and 8.5 µg/g (solid vector on Figure 4). Remarkably, these model concentrations are well within the Zr and Hf concentration ranges shown by unaltered DAM syenites and nepheline syenites (Figure 4). This leads to the conclusion that the Zr content in Ditrău 1 was tripled (400 µg/g to 1214 µg/g), whereas in Ditrău 2 it was more or less doubled (from 400 µg/g to 747 µg/g). This enrichment is also apparent in the very strong positive Zr anomalies shown in the trace element spider diagrams (Figure 3b,c). Logically, this holds true for the modal abundances of zircon as well, as this mineral is the only significant Zr and Hf carrier in the investigated rocks. Therefore, we conclude that the CL patchy zircon domains with Th/U > 15 and Th < 1000 µg/g (Figures 5–7, open small dots) are unlikely stemming from zircon growth from a siliceous melt, but represent voluminous late- to post-magmatic zircon growth due to the influx of a Zr-rich fluid during hydrothermal overprinting.

Using the Zr and Hf model concentrations (400 µg/g and 8.5 µg/g), the Zr saturation temperatures reduce to 808 ± 18 °C for Ditrău 1 and 754 ± 18 °C for Ditrău 2, which is consistent with an average Zr saturation temperature (789 ± 70 °C) calculated for the DAM felsic rocks [23]. One might argue that these temperatures have still to be taken as maximum Zr saturation temperatures, as the possible loss of alkalis during post-magmatic alteration might lead to a relative enrichment of Zr, thus again rendering the zircon saturation temperatures as too high. This possibility is invalidated by the fact that there is no negative correlation of Na_2O with Zr and Hf in all investigated rocks (Figure 4, inset), as would be expected if the Zr and Hf enrichment would only be a relative one. This also shows that the inferred post-magmatic hydrothermal event overprinting the "Magma2" syenites acted to different degrees on the rocks [23].

5.3. Zircon Th-U Systematics

The SIMS data reveal that the investigated samples have zircons with completely differing Th-U systematics (Figure 8). Ditrău 1 has igneous zircons exhibiting high Th/U ratios (Th/U > 15) due to comparably high Th concentrations (Th > 1000 µg/g), whereas Ditrău 2 zircons have Th/U < 5 at average Th and U concentrations (150–200 µg/g Th, 200–350 µg/g U, Th/U ~ approx. 0.65, [52]). Hydrothermally overprinted or newly grown zircons in both samples are strongly depleted in Th and U (Figure 8), pointing to the fact that the hydrothermal overprinting very effectively scavenged Th and U from the pre-existing igneous zircons and that newly grown zircon is virtually free of Th and U. The aberrant high Th concentrations (>4000 µg/g; Ditrau2_03a@1, 03a@2, 04@1, 22a@1) found for some SIMS spots from overprinted zircon domains are possibly due to contamination of the zircon SIMS measurement by Th-rich micro-inclusions, which were not identified by CL imaging at the available spatial resolution of ca. 200 nm, inasmuch as numerous LREE (light rare earth elements), Y, and Th-bearing mineral phases of varying sizes towards the rim were observed during the zircon preparation.

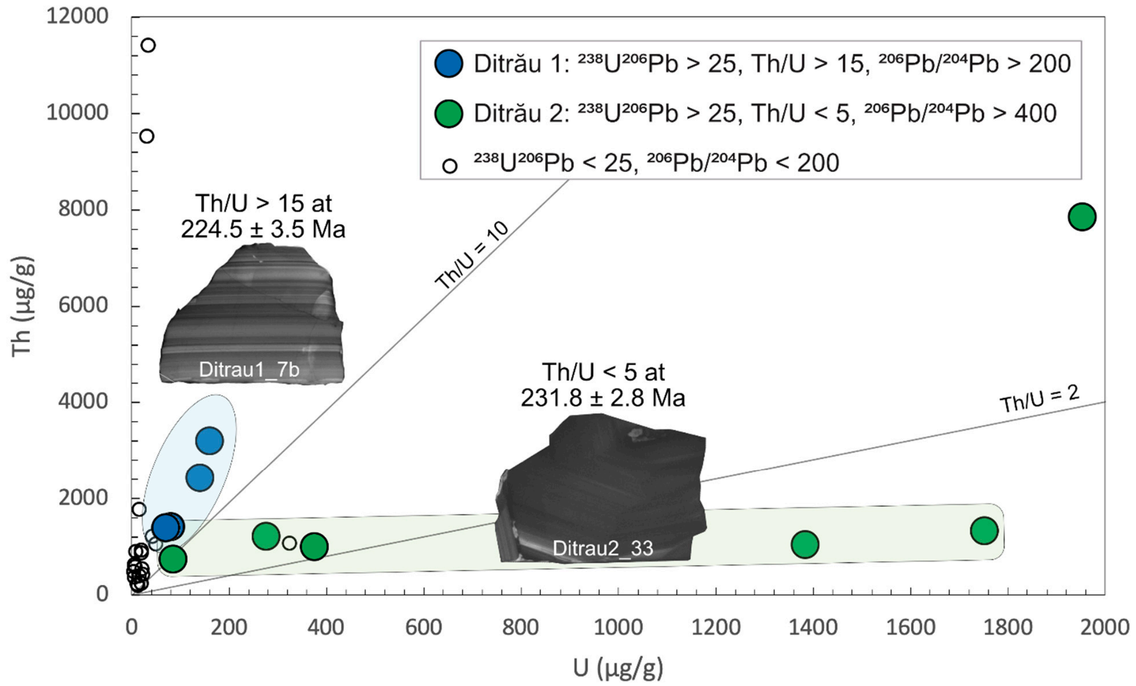

Figure 8. Plot of U versus Th showing the chemically different zircon domains relevant to the age interpretation (see Figure 5). Three trends can be identified: (1) SIMS pots from Ditrău 1 with $^{238}U/^{206}Pb > 25$, Th/U > 15, and $^{206}Pb/^{204}Pb > 200$ define a U-Pb concordia age of 224.5 ± 3.5 Ma (blue array). These spots are related to intermediate bright CL zircon domains with well-developed

oscillatory zonation. (2) SIMS spots from Ditrău 2 with $^{238}U/^{206}Pb > 25$, Th/U < 5, and $^{206}Pb/^{204}Pb > 400$ define a U-Pb age of 231.8 ± 2.8 Ma (green array). These spots are related to CL-dark zircon domains showing only a weakly visible oscillatory zonation. (3) The remaining SIMS spots from both samples with $^{238}U/^{206}Pb < 25$ and $^{206}Pb/^{204}Pb < 200$ (small, not colored) are attributed to strong U and Th loss during metasomatic/hydrothermal overprinting.

5.4. Zircon U-Pb Ages

Zircons from the investigated samples reveal textural and zonation features characteristic for both igneous and post-igneous hydrothermal replacement, recrystallization, and growth. The variability of zircon zonation varies from pure igneous oscillatory patterns (Figure 5, Ditrău 1 crystals 7b, 12a, Ditrău 2 crystals 22a, 33) to complete hydrothermal replacement or new growth (Figure 6, Ditrău 1 crystals 4, 5, and Ditrău 2 crystals 9, 10). It is thus likely that the post-magmatic overprinting event firstly partly modified the zircon's U-Pb systematics by recrystallization, and secondly has led to substantial growth of new zircon, thereby obscuring the primary magmatic zircon ages as delineated above (Sections 5.2 and 5.3). This is in line with observations showing that zircon precipitated from aqueous fluid is characterized by patchy to sigmoidal zonation patterns, elevated HFS and REE concentrations, and high non-radiogenic Pb contents [53].

This complex scenario is reflected in the linear arrays of the SIMS U-Pb data points (Figure 7a,c). Both arrays are interpreted as representing a binary mixture of two different Pb components, the first one denoting the purely radiogenic Pb from the magmatic stages and the second one a common Pb component which, within the estimated uncertainties, corresponds to a Stacey–Kramers model Pb at 230 Ma ($^{207}Pb/^{206}Pb = 0.851$ [50]). This is confirmed by calculating a three-dimensional regression plane through the two data arrays resulting in statistically identical initial $^{207}Pb/^{206}Pb = 0.833 \pm 0.027$ for Ditrău 1 and $^{207}Pb/^{206}Pb = 0.806 \pm 0.039$ for Ditrău 2, respectively. The forced regressions ($^{207}Pb/^{206}Pb = 0.851$) through all data points result in the lower intercept dates of 224.6 ± 3.5 Ma for Ditrău 1 and 230.3 ± 2.8 Ma for Ditrău 2 (Figure 7a,c). In both samples, the data are from the domains which exhibit a well-preserved magmatic oscillatory zonation (Figure 5) forming a tight cluster at $^{238}U/^{206}Pb > 25$ and $^{206}Pb/^{204}Pb > 200$. Neglecting these data points and calculating both a free and fixed regression through the remaining points results in lower intercept dates which are within the assigned uncertainties identical to the above ones. Therefore, we conclude that no new information can be gained from the data points with $^{238}U/^{206}Pb < 25$ and $^{206}Pb/^{204}Pb < 200$.

The five Ditrău 1 SIMS spots exhibiting $^{238}U/^{206}Pb > 25$ and $^{206}Pb/^{204}Pb > 200$ (Ditrau1_07b@1, 07b@2, 19@1, 19@2, 19@3) are from zircon domains which show a well-preserved magmatic oscillatory zonation (Figure 5, blue rings around yellow spot locations). Spot Ditrau1_19@3 is somewhat aberrant in having a comparably too-high $^{238}U/^{206}Pb$ and a low Th/U. The ^{207}Pb corrected concordia age of 224.5 ± 3.5 Ma (Figure 7b) calculated from the remaining four spots is interpreted as dating igneous zircon growth. This age is statistically identical to the above lower intercept discordia dates found for Ditrău 1.

The six Ditrău 2 SIMS spots with $^{238}U/^{206}Pb > 25$ and $^{206}Pb/^{204}Pb > 400$ (Ditrau2_02a@1, 04a@1, 08@3, 22a@1, 33@1, 33@2) are from zircon domains which also exhibit a preserved magmatic oscillatory zonation (Figure 5, green rings around yellow spot locations). Spot Ditrau2_22@1 is somewhat unusual in having a too-high Th/U when compared to all other spots having Th/U < 5. The ^{207}Pb corrected concordia age of 231.8 ± 2.8 Ma from the six spots (Figure 7d) is interpreted as dating igneous zircon growth. Again, this age is statistically identical to the above lower intercept discordia dates found for Ditrău 2.

Thus, both samples show no statistically significant age difference between the igneous zircon ages derived from the ^{207}Pb corrected data points and the lower intercept ages gained from regressing all data points. This leads us to conclude that the time of hydrothermal overprinting of both samples must either have taken place at a very late-magmatic or a very early post-magmatic stage, as otherwise a significant age difference between the purely igneous zircon growth and the hydrothermally common Pb contaminated zircons should be observable. In view of the uncertainty estimates for the concordia ages and lower intercept ages, this leads to the conclusion that the hydrothermal overprinting of the DAM alkaline rocks must have taken place within ca. 2 Ma after growth of the respective igneous zircons. Two independent hydrothermal events acting upon the DAM alkaline rocks have thus to be invoked, what is in contradiction to published scenarios speaking in favor of only one hydrothermal event (e.g., [16,26,29]).

To summarize, the Lăzarea suite sample Ditrău 1 has an igneous zircon growth age of 224.5 ± 3.5 Ma, whereas the Ghiduţ suite sample Ditrău 2 has an igneous zircon growth age of 231.8 ± 2.8 Ma. This age data interpretation as dating igneous zircon growth is well in line with the published zircon $\delta^{18}O$ isotope data which exhibit high values (syenites approx. 6.0–6.3‰, nepheline syenites approx. 5.1–5.3‰), characteristic for igneous temperatures and insignificant supra-crustal influence [23].

There are currently no thermobarometric models for zircon available for syenitic and nepheline syenitic rock compositions. Nevertheless, the thermobarometric models of [54,55] can be used to estimate the temperature ranges for Zr saturation and zircon growth in the investigated rocks. The aim of these model calculations is to derive some indication of when zircons are crystallized during the melt solidification process, i.e., what time point of the intrusion history is actually dated by the zircon growth ages. From the Zr-Hf whole-rock systematics, we concluded that Ditrău 1 has a modelled maximum Zr whole-rock concentration of ca. 900 µg/g (Figure 4). Applying thermobarometric models of zircon growth [54] shows the onset of zircon crystallization in Ditrău 1 to be at around 950 °C (at an estimated 0.6 GP and for an Si-poor A-type granite composition). This temperature is within the range of the liquidus of the Ditrău 1 melt and virtually identical to the estimated Zr saturation temperature of 953 ± 18 °C for the Ditrău 1 melt with 900 µg/g Zr (Table 1). This means that the zircon U-Pb age of ca. 225 Ma dates a relatively early part of the crystallization of the melt at or near the liquidus conditions. Zircon crystallization is then more or less complete at ca. 750 °C, a temperature well above the solidus of the melt at ca. 640 °C.

Taking the more realistic lower Zr whole-rock concentration (400 µg/g), the Zr saturation of the Ditrău 1 melt is substantially lowered to ca. 840 °C, meaning that zircon growth will have started at sub-liquidus conditions with ca. 70% melt present [54]. In this scenario, zircon growth is completed at ca. 700 °C, again well above the melt's solidus. The zircon age thus dates a later stage of melt crystallization, as is also suggested by the lower Zr saturation temperature of 808 ± 18 °C (Table 1). Whatever the Zr concentration in the Ditrău 1 melt was, the thermobarometric and geochemical modelling suggest that zircon grew early in the cooling history at temperatures above ca. 840 °C with at least 70% melt being present [54]. For the Ditrău 2 sample the maximum Zr whole-rock concentration is ca. 620 µg/g, and the resulting onset of zircon crystallization is then ca. 800 °C. The Zr saturation temperature estimate is 832 ± 18 °C, well in line with the former estimate. Using the same argumentation as above for a probably more realistic Zr content of ca. 400 µg/g, the same conclusions as for Ditrău 1 can be drawn.

Importantly, in both samples, zircon crystallization might have started immediately on the respective liquidus, but certainly, when still more than ca. 70 vol% melt was present. Therefore, both igneous zircon growth ages date a relatively early time point during melt crystallization. It also is worth mentioning that, due to the high alkalinity and the resulting high Zr solubility of the investigated rocks, no inherited zircons, for instance in the form of zircon cores, could be found.

5.5. Geochronological Implications

The most reliable published age data indicate that the emplacement of the DAM syenitic and gabbroic magmas was contemporaneous, and that the magmatic evolution of the DAM was "relatively short" [17]. These age data are based on isotope ages from the $^{40}Ar/^{39}Ar$, K/Ar, and Rb/Sr systems, with the ages given direct geochronological validity despite the limited precision of some of the analyses [20,35,40]. However, the inconsistencies, the absolute spread of the published age data, and the potential for disturbed Ar isotope systematics due to open-system behavior during tectonothermal overprinting make the evolutionary models for the DAM based on these ages "highly suspect" [31]. The postulated two- [35] or four-step magmatic evolution [36] starting in the Upper Triassic–Lower Jurassic and ending in the Middle Jurassic–Lower Cretaceous and covering at least 70 m.y. of magmatic activity seems highly improbable in view of the ambiguities in the underlying radiometric age data and the geodynamic evolution of the area during the Mesozoic and Cenozoic (see below).

Our new age data and recent published zircon and titanite U-Pb age data strongly contradict these findings. The authors of [6] report an in situ U-Pb age of titanite of 225.3 ± 2.7 Ma for a Lăzarea suite syenite sample. On the other hand, zircons from a syenite belonging to the Ghiduţ suite show an age of 232.4 ± 3.3 Ma. A Ditrău suite nepheline syenite sample exhibits U-Pb titanite and zircon ages of 230.6 ± 3.5 and 230.6 ± 2.4 Ma, respectively. Both the zircon as the titanite U-Pb ages are interpreted as mineral growth ages. A zircon upper intercept U-Pb age of a Ditrău syenite sample from Jolotca is 230.8 ± 3.3 Ma (recalculated from 229.6 + 1.7/−1.2 Ma using $^{238}U/^{235}U = 137.818$ [31,43]).

Talking into account only age data which can be unambiguously interpreted, i.e., which confidently date mineral growth and not arbitrary post-growth open-system process, we find that based on weighed mean ages combining the literature [6,31] and our data, at least three different magmatic events forming the alkaline rocks of the DAM can be distinguished (Figures 9 and 10):

- Event 1: intrusion of the Ghiduţ suite at 232.1 ± 0.8 Ma;
- Event 2: intrusion of the Ditrău suite at 230.7 ± 0.2 Ma;
- Event 3: intrusion of the Lăzarea suite at 224.9 ± 1.1 Ma.

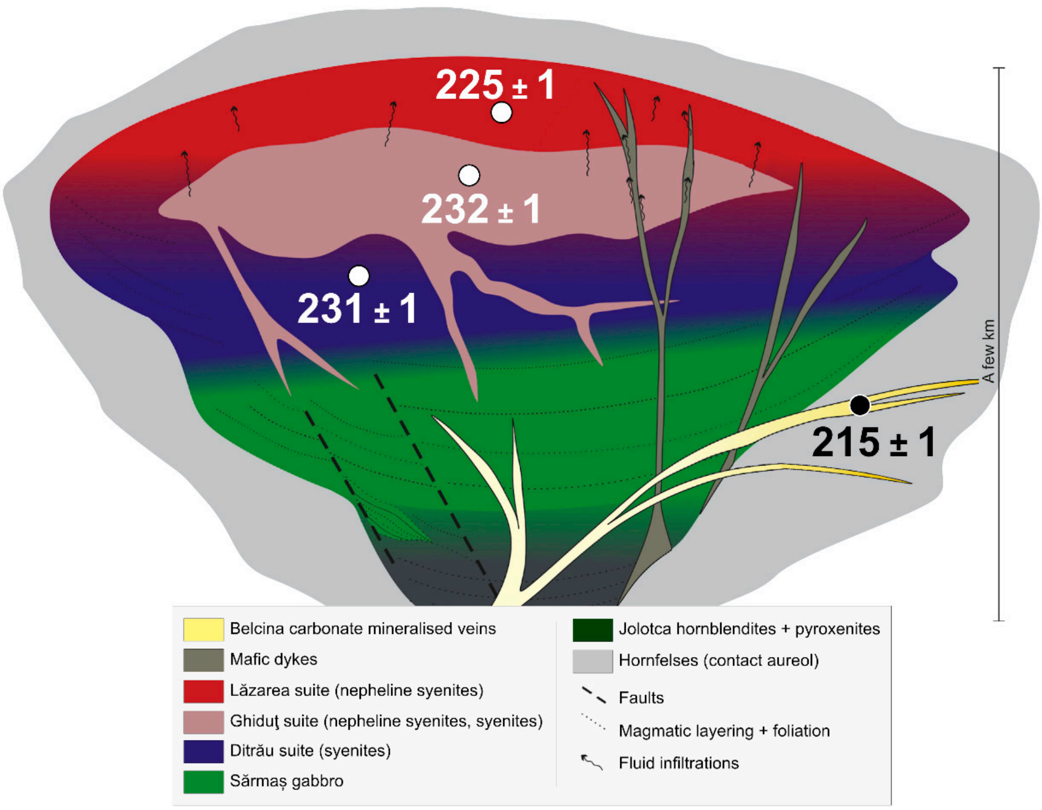

Figure 9. Schematic conceptual model of the Ditrău Alkaline Massif (modified from [17]) showing the inferred mean intrusion ages for the Ghiduţ suite (this work and [6]), the Lăzarea suite (this work and [6]), the Ditrău syenite [6,31], and the Belcina carbonate mineralized veins [56]. Color coding follows Figure 1.

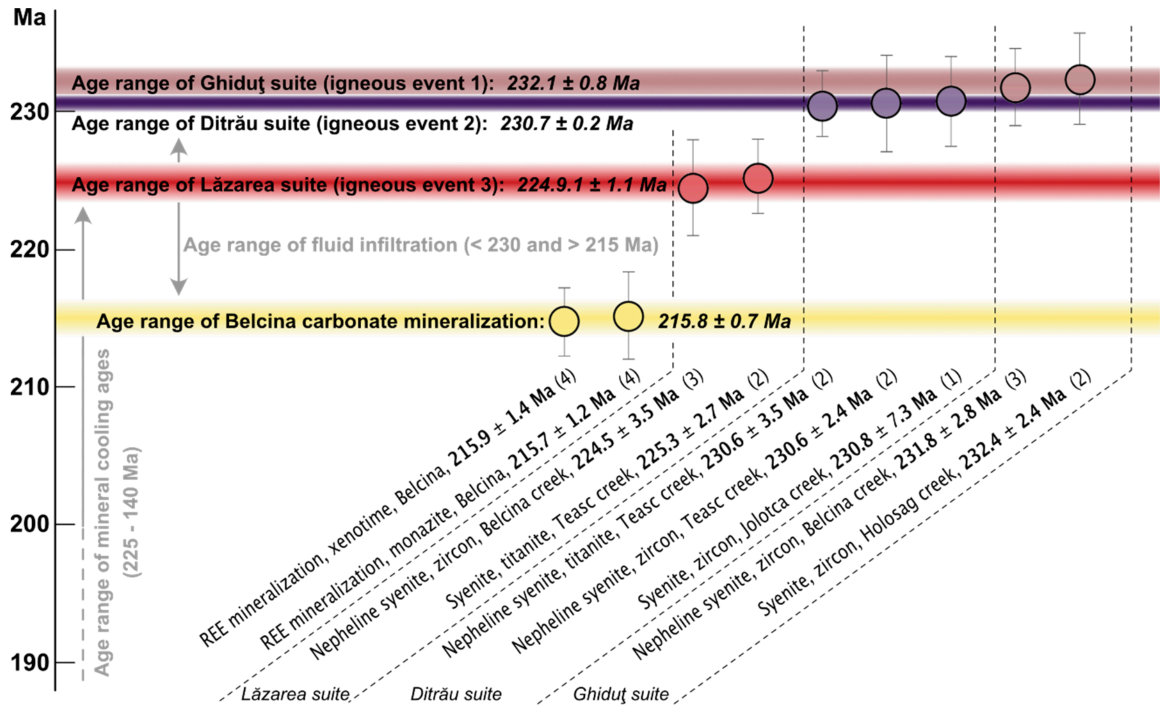

Figure 10. Compilation of inferred mean intrusion ages for the alkaline rocks of the DAM, the formation age of the Belcina carbonate mineralized veins, and the age ranges for metasomatic/hydrothermal overprinting and mineral cooling ages. Data are from (1) [31]; (2) [6]; (3) this work; (4) [56]. Color coding as in Figures 1 and 9.

On the base of our limited age data set we cannot decide solely whether the mean ages for the Ghiduţ suite (event 1) and the Ditrău suite (event 2) actually do represent two separate intrusion events. However, in view of the subtle differences in geochemical signatures of the two rock suites (Figure 3), the existence of a slight difference in the intrusion ages seems justified. By the term "intrusion", we understand the growth of zircon from a melt-crystal mush during the cooling and crystallization of the particular melts. As we cannot ascertain when the zircon growth actually takes place, i.e., pre-emplacement, during the emplacement, or post-emplacement, we use the term "intrusion" in a very general meaning.

On closer inspection of the zircon U-Pb age data from every particular igneous event, the Si-saturated syenitic samples are always older than the undersaturated nepheline syenite samples (Figures 9 and 10). Admittedly, the differences are partly within the reported analytical uncertainties, but nevertheless we take these age differences from the three igneous events as being significant. In view of the age data stemming from three different laboratories and dating methods, any issues with analytical accuracies can be safely ruled out. It thus seems possible that in every igneous event the syenites are older than the nepheline syenites by some 100,000 years. This is in line with field evidence of the intrusion sequences (e.g., [16,19–21,25,57]) suggesting the nepheline syenites as being younger than the syenites.

Based on the age systematics, the Lăzarea suite nepheline syenites cannot directly represent strongly altered Ghiduţ suite nepheline syenites (e.g., [21,25]), but are indeed formed by an independent magma batch, our igneous event 3, ca. 7 Ma (232–225 Ma) later than the intrusion of the Ghiduţ suite (igneous event 1). The authors of [17] interpreted the Lăzarea suite as a roof-zone intrusion, less evolved than the Ghiduţ suite and extensively altered, but the red color of the many Lăzarea suite samples not being indicative. We thus consequently propose that the Lăzarea suite forms an independent intrusion in the roof part of the DAM dated at ca. 225 Ma and definitely post-dating the intrusion of the Ghiduţ and Ditrău suites. The abundant Jolotca and Belcina vein mineralization [17,32,33] is tentatively dated at ca. 215 Ma in the Belcina carbonate mineralized vein system [57]. This provisional age obviously contradicts the traditional view that the fluids responsible for the REE-HFSE mineralization were identical to the ones overprinting the Lăzarea suite rocks, inasmuch as it is hardly conceivable that the fluids existed over a period of some 10 My.

The multigrain hornblende $^{39}Ar/^{40}Ar$ plateau ages from a gabbro and a diorite from the Sărmaș gabbro are 231.5 ± 0.1 Ma and 227.1 ± 0.1 Ma [40]. These were cautiously interpreted as dating relatively rapid cooling at high crustal levels following emplacement in the Middle to Upper Triassic, which is in line with our interpretation. For all other DAM rock types, no unambiguous age data exist. Therefore, for the moment we cannot put our age data into an unequivocal geochronological context with the DAM rocks in general. From the published geochemical and isotope geochemical data, it seems that the other DAM rock suites, e.g., Jolotca hornblendites and other ultrabasic rocks, the Sărmaș gabbro and Hagota alkali granites, are older (e.g., [16,20,36]). According to [23], the intrusion of mantle-derived phonolitic magma into the upper crust gave rise to the formation of nepheline syenites as the youngest rock suite. This is supported by the mantle like-isotopic composition of the alkaline melts and the relatively high (ca. 15 km) intrusion level [29], which would have protected the magma from crustal contamination. The present knowledge base seems to suggest a cessation in the igneous and/or hydrothermal activity after the intrusion of the Lăzarea suite and the onset of the vein-type carbonate mineralization being delayed by some 5 to 10 Ma later. Thus, the omnipresent hydrothermal/metasomatic overprinting of the DAM alkaline rocks [17,29] also has to be viewed as a multi-step process. As we could not attain any useful age data from the hydrothermal/metasomatic zircons, we can only suggest a time bracket for this overprinting event: the maximum age is ca. 232 Ma (the intrusion age of the Ghiduţ suite), the minimum age being ca. 215 Ma (age of the pristine Belcina carbonate vein mineralization [57]. However, according to [25] the veins are related to the Lăzarea suite, appearing indeed always nearby the Lăzarea suite. These relationships imply that the REE mineralization pre-dates the emplacement of the last-stage nepheline syenites. As yet, there are no absolute age data on these latest magmatic events, mostly dike-forming nepheline syenites. Therefore, these inferred relations cannot be independently ascertained at the moment.

5.6. Geological Implications

Our age data together with published data suggest that the intrusion of the DAM alkaline rocks took place in the Upper Triassic (232–225 Ma; Karnium-Norium). In view of the inferred field relations (e.g., [16,17,20,21,25]), this age range of igneous activity forming the DAM alkaline rocks possibly is also valid for the complete DAM. This short time interval provides the basis for a more realistic reconstruction of the igneous and geodynamic evolution of the DAM than the previously suggested formation time span of more than 70 m.y. [35,36]. Additionally, our age data do not provide any evidence for post-Norium igneous activity within the DAM. They are in excellent correspondence with the palinspastic reconstructions and petrogenetic models of the DAM [6,40]. Accordingly, the DAM was formed in an intraplate, rift-related extensional tectonic setting at the southwestern margin of the East European Craton during the Upper Triassic.

6. Conclusions

We report the first results of a petrochronological study of nepheline syenites from the Ghiduţ and the Lăzarea suites of the Ditrău Alkaline Massif (DAM) in the Eastern Carpathian Mountains in Romania. Based on field and geochemical evidence, the two rock suites are thought to represent the younger part of the DAM intrusives. Detailed zircon characterization, in situ zircon SIMS U-Pb dating, and geochemical modelling were used to establish the timing of zircon crystallization and thus to set time constraints on the igneous formation of these parts of the DAM.

Together with published geochemical and geochronological data three different magmatic events can be identified:

- Event 1: intrusion of the Ghiduţ suite at 231.1 ± 0.8 Ma;
- Event 2: intrusion of the Ditrău suite at 230.7 ± 0.2 Ma;
- Event 3: intrusion of the Lăzarea suite at 224.9 ± 1.1 Ma.

Although the ages of the events 1 and 2 are statistically indistinguishable, taking the geochemical and petrochronological data also into account, the mean ages for the three DAM suites can be interpreted as representing independent intrusion events. Each igneous event can tentatively be divided into older syenitic intrusion stages and younger nepheline syenitic ones, each with an age difference of some 100,000 years. No indication of any post 215 Ma igneous or hydrothermal activity is found, in contrast to the findings of former investigations which were solely based on mineral cooling ages.

The new data and interpretation significantly improve our understanding of the temporal and geochemical evolution of the DAM. In generalizing, we find that the formation time of the DAM, some 10 m.y., in association with multiple short-lived melt recharge and fractionation events, can be favorably compared with the formation time of more siliceous and less alkaline igneous complexes. On a first order, the formation times of small alkaline complexes, such as the DAM, and far larger igneous complexes, e.g., Adamello Batholith (Italy [7,9]), Fish Canyon Magmatic System (USA [8]), and Sesia Magmatic System (Italy [58,59]), are directly comparable. This then means that the underlying igneous processes, such as melt generation, assimilation, fractionation, and the duration of plumbing systems work on the same time scale for both sorts of magmatic rock suites.

Author Contributions: Conceptualization, U.K., J.B., G.J. and P.T.; Data curation, Q.-L.L. and Y.L.; Formal analysis, Q.-L.L.; Funding acquisition, J.B.; Investigation, U.K., J.B., G.J., L.I. and P.T.; Methodology, U.K., J.B., Q.-L.L., Y.L. and L.I.; Project administration, U.K., J.B. and P.T.; Resources, Q.-L.L. and Y.L.; Software, Y.L.; Supervision, U.K.; Validation, Q.-L.L. and Y.L.; Visualization, U.K. and J.B.; Writing—original draft, U.K. and J.B.; Writing—review and editing, U.K., J.B., Q.-L.L., G.J. and P.T. All authors have read and agreed to the published version of the manuscript.

Funding: The research activities of J.B. were co-financed by the funds granted under the Research Excellence Initiative of the University of Silesia in Katowice and are thankfully acknowledged. Q.L. acknowledges funding by the National Nature Sciences Foundation of China (Grant no. 41673059).

Institutional Review Board Statement: Not applicable.

Informed Consent Statement: Not applicable.

Data Availability Statement: The data presented in this study are available within the text.

Acknowledgments: Franz Biedermann (University of Vienna, Austria) is thanked for the help in sample preparation. We would like to thank the staff at the Beijing SIMS Laboratory (State Key Laboratory of Lithospheric Evolution, CAS, Beijing, China) for their invaluable help in acquiring the SIMS data. Moreover, we are thankful to the five anonymous reviewers for their helpful comments and suggestions. Open Access Funding by the University of Vienna is also highly appreciated.

Conflicts of Interest: The authors declare no conflict of interest. The funders had no role in the design of the study; in the collection, analyses, or interpretation of data; in the writing of the manuscript, or in the decision to publish the results.

References

1. Krumrei, T.V.; Villa, I.M.; Marks, M.A.W.; Markl, G. A ^{40}Ar/^{39}Ar and U/Pb Isotopic Study of the Ilímaussaq Complex, South Greenland: Implications for the ^{40}K Decay Constant and for the Duration of Magmatic Activity in a Peralkaline Complex. *Chem. Geol.* **2006**, *227*, 258–273. [CrossRef]
2. Biswal, T.K.; De Waele, B.; Ahuja, H. Timing and Dynamics of the Juxtaposition of the Eastern Ghats Mobile Belt against the Bhandara Craton, India; a Structural and Zircon U/Pb SHRIMP Study of the Fold-Thrust Belt and Associated Nepheline Syenite Plutons. *Tectonics* **2007**, *26*, TC4006. [CrossRef]
3. Pushkarev, E.V.; Ronkin, Y.L.; Yudin, D.S.; Travin, A.V.; Lepekhina, O.P. Age of the Formation of Nepheline Tilaite in the Uralian Platinum Belt; the Isotope Sm-Nd, Rb-Sr, U-Pb, (^{40}Ar/^{39}Ar, and K-Ar Datings and Their Limitations. *Dokl. Earth Sci.* **2014**, *455*, 312–316. [CrossRef]
4. Marks, M.A.W.; Markl, G. The Ilímaussaq Alkaline Complex, South Greenland. In *Layered Intrusions*; Charlier, B., Namur, O., Latypov, R., Tegner, C., Eds.; Springer: Dordrecht, The Netherlands, 2015; pp. 649–691. [CrossRef]

5. Borst, A.M.; Waight, T.E.; Finch, A.A.; Storey, M.; Le Roux, P.J. Dating Agpaitic Rocks: A Multi-System (U/Pb, Sm/Nd, Rb/Sr and $^{40}Ar/^{39}Ar$) Isotopic Study of Layered Nepheline Syenites from the Ilímaussaq Complex, Greenland. *Lithos* **2019**, *324–325*, 74–88. [CrossRef]
6. Pál-Molnár, E.; Kiri, L.; Lukács, R.; Dunkl, I.; Batki, A.; Szemerédi, M.; Almási, E.E.; Sogrik, E.; Harangi, S. Timing of Magmatism of the Ditrău Alkaline Massif, Romania—A Review Based on New U/Pb and K/Ar Data. *Central Eur. Geol.* **2021**, *64*, 18–37. [CrossRef]
7. Schoene, B.; Schaltegger, U.; Brack, P.; Latkoczy, C.; Stracke, A.; Günther, D. Rates of Magma Differentiation and Emplacement in a Ballooning Pluton Recorded by U–Pb TIMS-TEA, Adamello Batholith, Italy. *Earth Planet. Sci. Lett.* **2012**, *355–356*, 162–173. [CrossRef]
8. Wotzlaw, J.-F.; Schaltegger, U.; Frick, D.A.; Dungan, M.A.; Gerdes, A.; Günther, D. Tracking the Evolution of Large-Volume Silicic Magma Reservoirs from Assembly to Supereruption. *Geology* **2013**, *41*, 867–870. [CrossRef]
9. Schaltegger, U.; Davies, J.H.F.L. Petrochronology of Zircon and Baddeleyite in Igneous Rocks: Reconstructing Magmatic Processes at High Temporal Resolution. *Rev. Mineral. Geochem.* **2017**, *83*, 297–328. [CrossRef]
10. Krogh, T.E.; Kamo, S.L.; Robinson, P.; Terry, M.P.; Kwok, K. U-Pb Zircon Geochronology of Eclogites from the Scandian Orogen, Northern Western Gneiss Region, Norway: 14-20 Million Years between Eclogite Crystallization and Return to Amphibolite-Facies Conditions. *Can. J. Earth Sci.* **2011**, *48*, 441. [CrossRef]
11. Štípská, P.; Powell, R.; Hacker, B.R.; Holder, R.; Kylander-Clark, A.R.C. Uncoupled U/Pb and REE Response in Zircon during the Transformation of Eclogite to Mafic and Intermediate Granulite (Blanský Les, Bohemian Massif). *J. Metamorph. Geol.* **2016**, *34*, 551–572. [CrossRef]
12. Rubatto, D. Zircon: The Metamorphic Mineral. *Rev. Mineral. Geochem.* **2017**, *83*, 261–295. [CrossRef]
13. Burda, J.; Klötzli, U.; Woskowicz-Ślęzak, B.; Li, Q.-L.; Liu, Y. Inherited or Not Inherited: Complexities in Dating the Atypical 'Cold' Chopok Granite (Nízke Tatry Mountains, Slovakia). *Gondwana Res.* **2020**, *87*, 138–161. [CrossRef]
14. Höck, V.; Ionescu, C.; Balintoni, I.; Koller, F. The Eastern Carpathians "Ophiolites" (Romania): Remnants of a Triassic Ocean. *Ophiolites Relat. Geol. Balk. Reg.* **2009**, *108*, 151–171. [CrossRef]
15. Balintoni, I.; Balica, C.; Ducea, M.N.; Hann, H.-P. Peri-Gondwanan Terranes in the Romanian Carpathians: A Review of Their Spatial Distribution, Origin, Provenance, and Evolution. *Geosci. Front.* **2014**, *5*, 395–411. [CrossRef]
16. Jakab, G. *Geneza Masivului Alcalin Ditrău*; Mark House Printing: Gheorgheni, Romania, 2018; 166p.
17. Honour, V.C.; Goodenough, K.M.; Shaw, R.A.; Gabudianu, I.; Hîrtopanu, P. REE Mineralisation within the Ditrău Alkaline Complex, Romania: Interplay of Magmatic and Hydrothermal Processes. *Lithos* **2018**, *314–315*, 360–381. [CrossRef]
18. Anastasius, N.; Constantinescu, E. Tectostructural Position of the Foidic Rocks in the Romanian Carpathians. *Rev. Roum. Géologie* **1982**, *26*, 33–45.
19. Streckeisen, A. Das Nephelinsyenit-Massiv von Ditro (Siebenbürgen). II. Teil. *Schweiz. Mineral. Petrogr. Mitteilungen* **1954**, *34*, 336–409.
20. Streckeisen, A.; Hunziker, J. On the Origin of the Nephelinesyenite Massif of Ditró (Transylvania, Romania). *Schweiz. Mineral. Petrogr. Mitteilungen* **1974**, *54*, 9–77.
21. Morogan, V.; Upton, B.G.J.; Fitton, J.G. The Petrology of the Ditrău Alkaline Complex, Eastern Carpathians. *Mineral. Petrol.* **2000**, *69*, 227–265. [CrossRef]
22. Pál-Molnár, E.; Batki, A.; Almási, E.; Kiss, B.; Upton, B.G.J.; Markl, G.; Odling, N.; Harangi, S. Origin of Mafic and Ultramafic Cumulates from the Ditrău Alkaline Massif, Romania. *Lithos* **2015**, *239*, 1–18. [CrossRef]
23. Ódri, Á.; Harris, C.; Le Roux, P. The Role of Crustal Contamination in the Petrogenesis of Nepheline Syenite to Granite Magmas in the Ditrău Complex, Romania: Evidence from O-, Nd-, Sr- and Pb-Isotopes. *Contrib. Mineral. Petrol.* **2020**, *175*, 100. [CrossRef]
24. Streckeisen, A. Das Nephelinsyemt-Massiv von Ditro (Siebenbürgen), I. Teil. *Schweiz. Mineral. Petrogr. Mitteilungen* **1952**, *32*, 251–308.
25. Jakab, G. *Geologia Masivului Alcalin de La Ditrău*; Tipografia Alutus S.A.: Miercurea Ciuc, Romania, 1998; 57p.
26. Kovács, G.; Pál-Molnár, E. A Ditrói Alkáli Masszívum Granitoid Kőzeteinek Petrogenezise—Pedogenesis of Granitoid Rocks of the Ditrău Alkaline Massif (Transylvania, Romania). *Földt. Közlöny* **2005**, *135*, 121–143.
27. Shaw, R.; Goodenough, K.; Roberts, N.; Honour, V.; Horstwood, M.; Lenz, C. Timing and Source of Rare Earth Element Mineralisation in the Ditrău Alkaline Complex, Romania. *Appl. Earth Sci.* **2017**, *126*, 93. [CrossRef]
28. Batki, A.; Pál-Molnár, E.; Jankovics, M.É.; Kerr, A.C.; Kiss, B.; Markl, G.; Heincz, A.; Harangi, S. Insights into the Evolution of an Alkaline Magmatic System: An in-Situ Trace Element Study of Clinopyroxenes from the Ditrău Alkaline Massif, Romania. *Lithos* **2018**, *300–301*, 51–71. [CrossRef]
29. Fall, A.; Bodnar, R.J.; Szabó, C.; Pál-Molnár, E. Fluid Evolution in the Nepheline Syenites of the Ditrău Alkaline Massif, Transylvania, Romania. *Lithos* **2007**, *95*, 331–345. [CrossRef]
30. Batki, A.; Pál-Molnár, E.; Dobosi, G.; Skelton, A. Petrogenetic Significance of Ocellar Camptonite Dykes in the Ditrău Alkaline Massif, Romania. *Lithos* **2014**, *200–201*, 181–196. [CrossRef]
31. Pană, D.; Balintoni, I.; Heaman, L.M. Precise U-Pb Zircon Dating of the Syenite Phase from the Ditrău Alkaline Igneous Complex. *Stud. Univ. Babes-Bolyai Geol.* **2000**, *45*, 79–89.

32. Hîrtopanu, P.; Andersen, J.C.; Fairhurst, R. Nb, Ta, REE (Y), Ti, Zr, Th, U and Te Rare Element Minerals within the Ditrău Alkaline Intrusive Complex, Eastern Carpathians, Romania. Mineralogy of Székelyland, Eastern Transylvania, Romania. In *Mineralogy of Székelyland, Eastern Transylvania, Romania*; Szakáll, S., Kristály, F., Eds.; Csík County Nature and Conservation Society: Miercurea-Ciuc, Romania, 2010; pp. 89–128.
33. Hîrtopanu, P.; Andersen, J.C.; Fairhurst, R. Thorite, Thorogummite and Xenotime-(Y) Occurrence in Ditrău Alkaline Intrusive Massif, East Carpathians. *Proc. Romanian Acad. Sci. Ser. B* **2013**, *15*, 111–132.
34. Codarcea, A.; Codarcea-Dessila, M.; Ianovici, V. Structure Géologique Du Massif Des Roches Alcalines de Ditrau. *Révue Roum. Géologie Géophysique Géographie Géologie* **1958**, *1*, 1–135.
35. Pál-Molnár, E.; Árva-Sós, E. K-Ar Radiometric Dating on Rocks from the Northern Part of the Ditrău Syenite Massif and Its Petrogenetic Implication. *Acta Mineral. Petrogr. Szeged* **1995**, *36*, 101–116.
36. Kräutner, H.G.; Bindea, G. Timing of the Ditrau Alkaline Intrusive Complex (Eastern Carpathians, Romania). *Slovak Geol. Mag.* **1998**, *4*, 213–221.
37. Ionescu, J.; Tiepac, I.; Udrescu, C. Determination de l'âge Absolut Par La Metod Pb. *Inst. Geol St Tehn Ec Ser. B* **1966**, *44*, 55–63.
38. Bagdasarian, G.P. Despre Vîrsta Absolutà a Unor Roci Eruptive $i Metamorfice Din Masivul Ditráu, Muntii Banatului Din Romania. (A Study on the Absolute Age of Igneus and Metamorphic Rocks of the Ditró and the Bánát Hills.). *Stud. Cere Geol. Geofiz. Geogr. Ser. Geol.* **1972**, *17*, 13–21.
39. Minzatu, S.; Vajdea, E.; Romanescu, O.; Iosipenco, N. *K-Ar Ages of the Ditrau Massif*; IGG Bucureşti: București, Romania, 1981; 25p. (In Romanian)
40. Dallmeyer, D.R.; Kräutner, H.G.; Neubauer, F. Middle-Late Triassic 40Ar-39Ar Hornblende Ages for Early Intrusions within the Ditrău Alkaline Massif, Rumania. *Geol. Carpathica* **1997**, *48*, 347–352.
41. Liu, Y.; Li, Q.-L.; Tang, G.-Q.; Li, X.-H.; Yin, Q.-Z. Towards Higher Precision SIMS U-Pb Zircon Geochronology via Dynamic Multi-Collector Analysis. *J. Anal. At. Spectrom.* **2015**, *30*, 979–985. [CrossRef]
42. Burda, J.; Klötzli, U.; Majka, J.; Chew, D.; Li, Q.-L.; Liu, Y.; Gawęda, A.; Wiedenbeck, M. Tracing Proto-Rheic—Qaidam Ocean Vestiges into the Western Tatra Mountains and Implications for the Palaeozoic Palaeogeography of Central Europe. *Gondwana Res.* **2021**, *91*, 188–204. [CrossRef]
43. Vermeesch, P. IsoplotR: A Free and Open Toolbox for Geochronology. *Spec. ISSUE Front. Geosci. Tribute Prof. Xuanxue Mo.* **2018**, *9*, 1479–1493. [CrossRef]
44. Middlemost, E. Naming Materials in the Magma/Igneous Rock System. *Earth-Sci. Rev.* **1994**, *37*, 215–224. [CrossRef]
45. Le Maitre, R.W.; Streckeisen, A.; Zanetin, B.; Le Bas, M.J.; Bonin, B.; Bateman, P. *Igneous Rocks: A Classification and Glossary of Terms*, 2nd ed.; Cambridge University Press: Cambridge, UK, 2004; 273p.
46. Gervasoni, F.; Klemme, S.; Rocha-Júnior, E.R.V.; Berndt, J. Zircon Saturation in Silicate Melts: A New and Improved Model for Aluminous and Alkaline Melts. *Contrib. Mineral. Petrol.* **2016**, *171*, 21. [CrossRef]
47. Boehnke, P.; Watson, E.B.; Trail, D.; Harrison, T.M.; Schmitt, A.K. Zircon Saturation Re-Revisited. *Chem. Geol.* **2013**, *351*, 324–334. [CrossRef]
48. McDonough, W.F.; Sun, S. The Composition of the Earth. *Chem. Evol. Mantle* **1995**, *120*, 223–253. [CrossRef]
49. Pearce, J.A.; Harris, N.B.W.; Tindle, A.G. Trace Element Discrimination Diagrams for the Tectonic Interpretation of Granitic Rocks. *J. Petrol.* **1984**, *25*, 956–983. [CrossRef]
50. Stacey, J.S.; Kramers, J.D. Approximation of Terrestrial Lead Isotope Evolution by a Two-Stage Model. *Earth Planet. Sci. Lett.* **1975**, *26*, 207–221. [CrossRef]
51. Watson, E.B.; Harrison, T.M. Zircon Saturation Revisited: Temperature and Composition Effects in a Variety of Crustal Magma Types. *Earth Planet. Sci. Lett.* **1983**, *64*, 295–304. [CrossRef]
52. Kirkland, C.L.; Smithies, R.H.; Taylor, R.J.M.; Evans, N.; McDonald, B. Zircon Th/U Ratios in Magmatic Environs. *Lithos* **2015**, *212–215*, 397–414. [CrossRef]
53. Corfu, F.; Hanchar, J.M.; Hoskin, P.W.O.; Kinny, P.D. Atlas of Zircon Textures. *Rev. Mineral. Geochem.* **2003**, *53*, 469–500. [CrossRef]
54. Kirkland, C.L.; Yakymchuk, C.; Olierook, H.K.H.; Hartnady, M.I.H.; Gardiner, N.J.; Moyen, J.-F.; Hugh Smithies, R.; Szilas, K.; Johnson, T.E. Theoretical versus Empirical Secular Change in Zircon Composition. *Earth Planet. Sci. Lett.* **2021**, *554*, 116660. [CrossRef]
55. Kelsey, D.E.; Clark, C.; Hand, M. Thermobarometric Modelling of Zircon and Monazite Growth in Melt-Bearing Systems: Examples Using Model Metapelitic and Metapsammitic Granulites. *J. Metamorph. Geol.* **2008**, *26*, 199–212. [CrossRef]
56. Klötzli, U.; Burda, J.; Tibuleac, P. Dating the REE Mineralization in the Ditrău Alkaline Massif, Romania. *Minerals* **2022**. submitted.
57. Pál-Molnár, E.; Batki, A.; Ódri, Á.; Kiss, B.; Almási, E. Geochemical Implications for the Magma Origin of Granitic Rocks from the Ditrău Alkaline Massif, Eastern Carpathians, Romania. *Geol. Croat.* **2015**, *68*, 51–66. [CrossRef]
58. Klötzli, U.S.; Sinigoi, S.; Quick, J.E.; Demarchi, G.; Tassinari, C.C.G.; Sato, K.; Günes, Z. Duration of Igneous Activity in the Sesia Magmatic System and Implications for High Temperature Metamorphism in the Ivrea-Verbano Deep Crust. *Lithos Oslo* **2014**, *206–207*, 19–33. [CrossRef]
59. Sinigoi, S.; Quick, J.E.; Demarchi, G.; Klötzli, U.S. Production of Hybrid Granitic Magma at the Advancing Front of Basaltic Underplating; Inferences from the Sesia Magmatic System (Southwestern Alps, Italy). *Lithos Oslo* **2016**, *252–253*, 109–122. [CrossRef]